Computers and Fluids 283 (2024) 106407

Contents lists available at ScienceDirect

Computers and Fluids

journal homepage: www.elsevier.com/locate/compfluid

Review

Port-Hamiltonian formulations for the modeling, simulation and control of fluids

Flávio Luiz Cardoso-Ribeiro [a,b,*], Ghislain Haine [b], Yann Le Gorrec [c], Denis Matignon [b], Hector Ramirez [d]

[a] Divisão de Engenharia Aeronáutica e Aeroespacial, Instituto Tecnológico de Aeronáutica, São José dos Campos, 12228-900, SP, Brazil
[b] Fédération ENAC ISAE-SUPAERO ONERA, Université de Toulouse, Toulouse, 31055, France
[c] SUPMICROTECH, CNRS, FEMTO-ST institute, Besançon, 25000, France
[d] Departamento de Electrónica, Universidad Técnica Federico Santa María, Valparaiso, 2390123, Chile

ARTICLE INFO

Keywords:
Energy-based modeling
Port-Hamiltonian systems
Structure-preserving discretization
Boundary control
Shallow water equations
Incompressible Navier–Stokes equations

ABSTRACT

This paper presents a state of the art on port-Hamiltonian formulations for the modeling and numerical simulation of open fluid systems. This literature review, with the help of more than one hundred classified references, highlights the main features, the positioning with respect to seminal works from the literature on this topic, and the advantages provided by such a framework. A focus is given on the shallow water equations and the incompressible Navier–Stokes equations in 2D, including numerical simulation results. It is also shown how it opens very stimulating and promising research lines towards thermodynamically consistent modeling and structure-preserving numerical methods for the simulation of complex fluid systems in interaction with their environment.

Contents

* Corresponding author.
E-mail address: flaviocr@ita.br (F.L. Cardoso-Ribeiro).

https://doi.org/10.1016/j.compfluid.2024.106407
Received 29 November 2023; Received in revised form 18 July 2024; Accepted 31 July 2024
Available online 20 August 2024

Introduction

Port-Hamiltonian (pH) systems formulations are an extension of Hamiltonian formulations initially proposed in the context of classical mechanics for closed systems to model open physical systems. These energy-based formulations encode through a well-defined geometric structure the links existing between the dynamics of the energy variables, the thermodynamic driving forces, the energy function and the environment using the notion of ports of interaction. They are then particularly well suited for the modular modeling of complex multi-physics systems. These formulations have recently been generalized to distributed parameters systems in [135] defining the notion of boundary port variables from the evaluation of the co-states variables at the boundary of the spatial domain. They have been extensively used in continuous mechanics to model flexible/compliant structures such as beams or plates. Their application to the modeling of fluids, as systems with possible interactions with the environment through open flows or fluid structure interactions is more recent but has shown to be very interesting for both modeling and simulation purposes in various fields of application such as aeronautics, acoustics, microfluidic systems, process control. There are indeed a lot of structure-preserving numerical schemes that have been developed to preserve the energy balances and to avoid the numerical stiffness due to the interdomain couplings between different subsystems. In this paper, we give an overview of these recent results, focusing on their applications to fluid dynamics in general and to some well-known application cases such as shallow water equations or incompressible Navier–Stokes equations. We also give some open research lines that are currently investigated in this field of research.

The paper is organized as follows: a comprehensive state of the art is presented in Section 1, with an emphasis on structure-preserving numerical methods for partial differential equations (PDE). Then, in Section 2, pH modeling in fluids mechanics is addressed: a general setting is presented and possible extensions to dissipative pH systems are introduced; moreover two motivating examples are treated, which will be of interest throughout the paper, the shallow water equation (SWE) in Section 2.3 and the incompressible Navier–Stokes equation (NSE) in Section 2.4. In Section 3, the structure-preserving discretization method called Partitioned Finite Element Method (PFEM) is detailed on the worked out example of the 2D SWE, in the irrotational and non-dissipative case; then it is shown how dissipation can be taken into account at the discrete level in a structure-preserving manner; finally, the control of the 2D SWE by boundary feedback helps illustrate the effectiveness of the approach. The example of the 2D incompressible NSE is presented as a more difficult example, and first rephrased into a linear pH system, when the choice is made to describe it with vorticity as energy variable, and stream function as co-energy variable; convincing numerical results are provided for 3 different values of the Reynolds number on the benchmark of the lid-driven cavity problem. Finally, in Section 4, an extension of the approach, including thermodynamics, is addressed: first in Section 4.1, quasi pH systems are presented, when the dynamical system depends on the co-energy variables instead of a modulation by the energy variables; finally in Section 4.2, the formalism of irreversible pH system is introduced.

1. State of the art

Since the topic addressed in this review paper bears strong links with several scientific fields, the comprehensive review will be organized under the following scientific themes of interest: some cornerstone publications on pH systems will be presented first, immediately followed by a list of worked-out applications of this approach. Then, the focus will be made on Hamiltonian formulations available in fluid mechanics. The most detailed part is devoted to so-called compatible discretization. Finally, some links to thermodynamics are provided.

Port-hamiltonian systems. A complete and comprehensive framework for modeling the dynamics of complex interconnected systems as pH systems can be found first in [43] and later in [133]: in both these books, infinite-dimensional systems are tackled, but not only. The seminal paper that presents distributed-parameter systems as pH systems for the first time is [135]; since then, many extensions and novelties have been explored, which are extensively traced back in the literature review paper [119]. In particular, this approach is based on *Hamiltonian systems* for closed physical systems, see [106], and on the abstract notion of *Dirac structures*, defined in [38], for open physical systems. One of the main properties of pH systems is their invariance under power-conserving interconnection, detailed in [34]. The particular 1D case has been fully understood from the original work [83], dissipation has been taken into account in [139] thanks to the introduction of extra dissipative ports, and [73] is a monograph on the 1D linear case: existence, uniqueness and regularity results are given in these references. For the nD case, such theoretical results can be found in [80] for the wave equation, a generalization to other first-order operators linear systems is proposed in [127], and a generalization to first- and second-order operators linear systems encompassing the previous one can be found in [22]; a more abstract setting via system nodes is provided in [112]. In particular in 2D, the geometric setting has been extended to tensor-valued functionals, see [18]. In [140], the symmetry reduction of a pH system is proved to give rise to another pH system in a smaller space dimension, which is another very interesting property of pH system for the modeling of multiscale systems. Preserving the pH structure through Model Order Reduction also proves possible, as has been studied, for instance in [63]; a more recent work in this direction, focusing on the realization of pH systems in a data-driven manner can be found in [12]. Finally, note that the link between infinite-dimensional pH systems and the GENERIC[1] framework, which helps encode the first and second laws of thermodynamics, has been given in [86,102].

Some worked-out examples. Many references put forward the interest of the modular approach enabled by pH systems: let us mention [5] for a rotating flexible spacecraft, or [142] for the dynamics of complex mechanical structures where, typically, subsystem dynamics can be formulated in a domain-independent way and interconnected by means of power flows. In [70], the 1D longitudinal vibrations of a nanorod are modeled as a differential–algebraic pH system. Now, the reader interested in examples involving fluid mechanics models will have quite a wide choice also: the 1D SWE has been presented in [68,69] where a network of irrigation channels is modeled and controlled by interconnection, an extension to 2D can be found in [109], using the language of exterior calculus and differential forms. The 2D SWE has also been studied in [28] together with boundary control of a circular water tank. Coupled systems of Fluid–Structure Interaction (FSI) have been extensively studied in 1D in [32] for a liquid sloshing in a moving container, then generalized in 2D in [33]; note that these latter works use vector calculus, in many available coordinate systems, instead of exterior calculus. In [4] one can find a derivation of the 1D NSE coupled

[1] the acronym stands for *General Equation for the Non-Equilibrium Reversible–Irreversible Coupling*

with chemical reactions. Moreover, quite a number of examples are applied either to vocal folds, see *e.g.* [97,98], or to musical instruments, typical for multi-physics problem, see *e.g.* [87] where the jet interacting with the brass player's lip is modeled as a pH system, and also [121] where the guitar is modeled as a pH system resulting from FSI. A careful derivation of a poro-elastic model can be found in [3]. The thermo-magneto-hydrodynamics (TMHD) interdomain couplings is studied in depth in [105] for plasma high confinement in Tokamaks.

Hamiltonian formulations in fluid mechanics. The solutions to systems of PDEs such as the NSE satisfy strong constraints, which reflect the underlying mathematical structure of the equations (*e.g.*, Hamiltonian structure, Poisson structure, de Rham sequence). The seminal paper on such a structured viewpoint is [101]. The modeling of gas flow, based on the Euler equations, is fully reported in e.g. [41]. A first description of NSE as a pH system can be found in 1D in [4], and in ND in [96]. A more geometric-oriented description of the NSE has been proposed in [25], a work based on the companion papers [117,118]. Recently, the same authors introduced an extension of their framework to thermodynamics with an application to Fourier–Navier–Stokes fluid in [27], and also to FSI in [26]. All these works are based on the classical derivation of the equations of fluid mechanics, which can be found in the monographs [16,35].

Compatible discretization. One of the best expositions of this central topic can be found in [143]: *In recent years, there has been an increasing interest in the various aspects of structure preservation at the discrete level. This interest is rooted in three important points. First, there are well-known connections between discrete structure preservation and standard properties of numerical methods. Second, standard properties only guarantee physical fidelity in the limit of fully (at least highly) resolved discretizations. Reaching this limit requires infeasible computational resources. In contrast, structure-preserving discretizations, by construction, generate solutions that satisfy the underlying physics even in highly under-resolved simulations. This is extremely relevant since most (if not all) simulations are inherently under-resolved. Third, physics preservation is fundamental when coupling systems in multi-physics problems. The underlying principle behind structure-preserving discretizations is to construct discrete approximations that retain as much as possible the structure of the original system of PDEs. A departure from this principle introduces spurious nonphysical modes that pollute the physics of the system being modeled.*

General presentation of this topic can be found in [14,71]. With this main concern of compatible discretization at stake, many different flavors have been presented: the first structure-preserving discretization scheme for distributed pH systems was proposed by [60], where the authors proposed a mixed finite element method for the 1D wave equation; the method used a low-order Whitney bases function and was based on exact satisfaction of the strong-form equations in the corresponding spanned finite-dimensional approximation spaces. Based on this, [110] presented a structure-preserving numerical scheme for the nonlinear SWE, which proves useful since both mass and energy are preserved at the discrete level. An extension of this method to use the higher order pseudo-spectral polynomial approximation basis was then proposed by [103], and the Bessel function was used by [141]. A similar idea was considered by [50–52] for the 1D linear transmission line and the Maxwell equations. There, one equation was kept in the strong form, and the other in the weak form. All these previous methods, which rely on finding compatible bases that exactly satisfy at least one of the equations in strong form, are relatively straightforward to apply for 1D equations. However, they seem cumbersome for higher dimension. Using rather the weak form of both equations, and two different types of basis functions for flows and efforts were studied in [77] and applied for the 2D wave equation, requiring a projection in the very last step. A comprehensive overview of this type of method can be found in the monograph [76]. An adaptation of the finite difference method to pH systems both in 1D and 2D can be found in [130], where the pH framework is combined with finite differences on staggered grids to derive control oriented reduced order systems for the 2D wave equation.

Discrete exterior calculus (DEC), see [94] and references therein, has been applied to pH system in [126]. Finite element exterior calculus (FEEC), with the seminal papers [6,7], has recently been applied to pH system in [24], also inspired by the dual-field mixed weak formulation introduced in [143]. The primal–dual setting is also a key point in [129]. And a full review of the subject of compatible finite elements for geophysical fluids can be found in [37]. More recently, another approach has developed a discretization of the physical field laws based on discrete variational principles: this approach has been used in the past to construct variational integrators for Lagrangian systems, see e.g. [54]. Also, structure-preserving schemes applied to the GENERIC framework have been explored by [78]. Tackling dissipative evolution equations in a structure-preserving way has been studied by [46].

In a nutshell, the Partitioned Finite Element Method (PFEM) is based on the mixed finite elements method for first-order coupled systems, an integration by parts or the appropriate Stokes formula to make the boundary control appear naturally, and also the finite element method to take into account the constitutive relations linking energy variables to co-energy variables; it comes along with sparse matrices which might help a lot for the scientific computing aspect. Thus, this method is based on classical applied mathematics theories, which are fully developed in the monographs [15,59]. A first global presentation of the PFEM can be found in [30]. The PFEM has already enjoyed many successful examples where the dynamics is linear and the Hamiltonian quadratic: the 2D wave equation [125], an extension to the damped case [123], the nD heat equation [124], the 3D or 2D Maxwell equations [66,111], the Reissner–Mindlin plate [18], the Kirchhoff–Love plate [19] for example. The extension to some implicit pH system, like the Dzektser seepage model in 2D or the nanorod in 1D, are to be found in [9]. When mixed boundary controls are to be taken into account, different adaptations of the PFEM can be used, see [20], or [21] for the use of the Hellinger–Reissner principle. Note that a full characterization of the optimal choice of finite elements families based on the numerical analysis of the scheme, together with worked out simulation results for the 2D wave equation on different geometries, is available in [67]; in particular, the importance of the discrete de Rham complex is enlightened. As a convincing example of the advantage of developing structure-preserving numerical methods for coupled subsystems, one can cite [65], in which some refined asymptotics, that were predicted theoretically at the continuous level, can be recovered at the discrete level. However, the application of the PFEM to fluid mechanics requires some care, since the dynamical system is intrinsically non-linear: nevertheless, as will be detailed in this paper, it can be extended to these models, either when the non-linear relation proves of polynomial nature [28], or when the constitutive relation, though linear, becomes of differential nature [64]. Last, but not least, the PFEM comes along with a user guide [23,53], and the source codes are made available at https://g-haine.github.io/scrimp/. In this respect, a useful benchmark on numerical models for pHs can be found at https://algopaul.github.io/PortHamiltonianBenchmarkSystems.jl/.

About differential algebraic equations. In the classical energy-coenergy formulation of pH system, the dynamic equations are supplemented by the so-called constitutive relations, which do play the role of constraints. As far as coupling is concerned in modeling civil engineering structures, a representation of the interconnected systems is used to generate coupling constraints, which leads to differential algebraic equations (DAEs) of index at most two. [79] is one of the first monographs on these kinds of equations. Infinite-dimensional setting for DAE has been tackled in [82], while the pH formulation has been studied in [40]. A strong link between pHs and DAEs has been fully detailed in [131]. The general definition of so-called finite-dimensional descriptor pH system followed in [8]. [136] provides a closer look at such

systems with many examples, and in particular both the Lagrange subspace and Dirac structure are introduced. The works [91,138] and recently [92] testify of the specific interest in dissipative pH-DAEs, which are more likely to appear in the modeling of real-world processes. A full review on the subject of DAEs has been published in [90]. Recently, there has been a renewed interest in infinite-dimensional DAEs with the question of solvability addressed in [72], the Weierstraßcanonical form in [48], and the notion of index in [49].

The role of thermodynamics. In numerous physical scenarios, thermal aspects and irreversible thermodynamic processes play a crucial role. This is particularly evident in heat transfer, chemical reactions and reacting fluids, among others [13,39]. The dissipative pH system formulation can fall short in these instances, necessitating the integration of heat or entropy balance equations into the models. Modeling, simulation and control challenges in chemical engineering are notably complex due to nonlinearities arising from thermodynamic properties and flux relationships [42]. A promising method for creating nonlinear controllers involves leveraging the characteristics of dynamical models based on fundamental principles. These include symmetries, invariants, and balance equations related to specific thermodynamic potentials, like entropy. In many fluid systems, these balance equations have been effectively applied as dissipation inequalities [36,68] in passivity-based control schemes, now a well-established area of study [43]. For chemical processes, different thermodynamic potentials such as the entropy or Helmholtz free energy are considered in designing controllers based on Lyapunov functions and passivity [2]. However, developing constructive structure preserving methods for numerical approximations in this context remains a challenge. Several types of "thermodynamic" dynamical models have been proposed, aiming to account for both energy conservation and irreversible entropy production. These include pseudo-gradient systems [96], which are redefined with a pseudo-metric, similar to the approach for electrical circuits in [17]. Other types include metriplectic systems such as the General Equation for the Non-Equilibrium Reversible–Irreversible Coupling GENERIC [61,62,108], nonlinearly constrained Lagrangian systems [55,93], and implicit Hamiltonian control systems [44,104,115,116], defined on submanifolds of thermodynamic phase spaces or their symplectic extensions, and controlled by systems on contact manifolds or their symplectizations [137]. More recently a non-linear extension of pH systems with a clear underlying geometric structure has been proposed to cope with both the first and second laws of Thermodynamics, namely Irreversible pH (IpH) systems [115,116].

2. Port-Hamiltonian modeling of fluid mechanics

2.1. General setting

In what follows, we consider fluids filling a spatial domain denoted Ω defined by the spatial coordinate $\boldsymbol{\zeta}$ and boundary $\partial\Omega$. We denote by $H(\Omega)$ the Sobolev space of weakly differentiable functions, and by $\mathcal{X} \subset H(\Omega)$, the space of state variables. Infinite-dimensional pH systems formulation consists in writing balance equations on extensive variables of thermodynamics, *i.e.* the energy variables, as a function of the corresponding intensive variables of thermodynamics, *i.e.* the co-energy variables, derived from the variational derivative of the energy. When the constitutive relations linking the state and co-state variables are linear, and when only conservative phenomena are considered, it leads to a system of PDEs of the form $\partial_t \boldsymbol{x}(\boldsymbol{\zeta},t) = \mathcal{J}\delta_{\boldsymbol{x}}\mathcal{H}$ where $x(\boldsymbol{\zeta},t) \in \mathcal{X}$ is the state, $\mathcal{J}$ is a formally skew symmetric differential operator defined over Ω and $\mathcal{H}$ the total energy of the system defined by:

$$\mathcal{H} := \int_\Omega \mathscr{H}(\boldsymbol{x})\,\mathrm{d}\,\Omega, \tag{1}$$

where $\mathscr{H} : \mathcal{X} \to L^1(\Omega,\mathbb{R})$ is the energy density. PH formulations also allow to explicit, in the case of open physical systems, the links existing between the dynamics of the system, the energy and the power flow at the boundary of the spatial domain, as stated in Definition 1.

Definition 1. A distributed-parameter pH system is defined by the set of PDEs and boundary port variables defined by:

$$\partial_t \boldsymbol{x}(\boldsymbol{\zeta},t) = \mathcal{J}\delta_{\boldsymbol{x}}\mathcal{H}, \ (\text{or } \boldsymbol{f} = \mathcal{J}\boldsymbol{e}), \tag{2}$$

$$\begin{pmatrix} \boldsymbol{f}_\partial \\ \boldsymbol{e}_\partial \end{pmatrix} = \mathcal{W}_{\partial\Omega}\,\delta_x\mathcal{H}, \tag{3}$$

where $\mathcal{J}$ is a formally skew-symmetric differential operator, known as the structure (matrix) operator, $\boldsymbol{f}_\partial$ and $\boldsymbol{e}_\partial$ are the boundary flow and effort port variables, $\mathcal{W}_{\partial\Omega}$ is an operator that is related to the normal and tangential projections on $\partial\Omega$ of the co-energy variables $\boldsymbol{e} := \delta_{\boldsymbol{x}}\mathcal{H}$ induced by $\mathcal{J}$ such that:

$$\dot{\mathcal{H}} = \int_{\partial\Omega} \boldsymbol{f}_\partial \cdot \boldsymbol{e}_\partial\,\mathrm{d}\gamma, \tag{4}$$

where $\dot{\mathcal{H}}$ denotes the time derivative of the Hamiltonian, and $\int_{\partial\Omega} \boldsymbol{f}_\partial \cdot \boldsymbol{e}_\partial\,\mathrm{d}\gamma$ describes the power supplied to the system through the boundaries.[2]

From a geometrical point of view, $(\boldsymbol{f},\boldsymbol{e},\boldsymbol{f}_\partial,\boldsymbol{e}_\partial) \in \mathcal{D}$ at any time $t > 0$, where $\mathcal{D}$ is a Dirac structure[3].

From (4) one can see that the total energy of the system is constant along the state trajectories as soon as the boundary port variables are set to zero, *i.e.* when the system is closed with respect to energy. This reflects the fact that the considered system is conservative, and balance equations reduce to a system of conservation laws. When the system is subject to internal dissipation, as it is the case for fluids with viscous damping, it is possible to extend the Dirac structure with some dissipative ports associated to dissipative closure relations as detailed in the next section. An alternative approach that will be discussed in Section 4 is to include in the system description the thermal domain. PH formulations have also been recently extended to systems with constraints or implicit definitions of the energy in [89]; boundary-implicit port-Hamiltonian systems have been thoroughly treated in the thesis [99].

2.2. Dissipative port-Hamiltonian systems

As it is the case for finite-dimensional systems, infinite-dimensional pH formulations initially proposed to represent conservative systems have been extended in [139] to systems with dissipation of the form $\partial_t \boldsymbol{x}(\boldsymbol{\zeta},t) = \mathcal{J}\delta_{\boldsymbol{x}}\mathcal{H} - \mathcal{G}S\mathcal{G}^*\delta_{\boldsymbol{x}}\mathcal{H}$, where $\mathcal{G}$ is a differential operator and $\mathcal{G}^*$ the corresponding formal adjoint, and $S \geq 0$ is a non-negative bounded matrix operator of appropriate dimensions. In this case, $\mathcal{G}S\mathcal{G}^*$ represents the dissipation and can be split into two parts such as to extend the Dirac structure, as stated in Definition 2.

Definition 2. A distributed-parameter dissipative pH system is defined by the set of PDEs and boundary port variables defined by:

$$\begin{pmatrix} \partial_t \boldsymbol{x}(\boldsymbol{\zeta},t) \\ \boldsymbol{f}_d \end{pmatrix} = \underbrace{\begin{bmatrix} \mathcal{J} & \mathcal{G} \\ -\mathcal{G}^* & 0 \end{bmatrix}}_{\widetilde{\mathcal{J}}} \begin{pmatrix} \boldsymbol{e} \\ \boldsymbol{e}_d \end{pmatrix}, \ \text{with } \boldsymbol{e}_d = S\boldsymbol{f}_d, \tag{5}$$

$$\begin{pmatrix} \boldsymbol{f}_\partial \\ \boldsymbol{e}_\partial \end{pmatrix} = \widetilde{\mathcal{W}}_{\partial\Omega} \begin{pmatrix} \boldsymbol{e}|_{\mathrm{d}\,\Omega} \\ \boldsymbol{e}_d|_{\mathrm{d}\,\Omega} \end{pmatrix}, \tag{6}$$

where $\partial_t \boldsymbol{x}(\boldsymbol{\zeta},t) \in \mathcal{F}$ and $S > 0$. $\widetilde{\mathcal{J}}$ is an extended formally skew-symmetric differential operator, $\boldsymbol{f}_\partial$ and $\boldsymbol{e}_\partial$ are the boundary flow and effort port variables, $\widetilde{\mathcal{W}}_{\partial\Omega}$ is an operator induced by $\widetilde{\mathcal{J}}$, that is related to

[2] In this work, we will always assume a strong regularity (*i.e.* at least C^1 in space and time) for the solutions to a pH system. In this case, the boundary traces of such solutions are then sufficiently regular to allow the identification of the duality bracket at the boundary of Ω with the L^2-inner product at the boundary.

[3] Some useful definitions are recalled in Appendix A, see also *e.g.* [83]

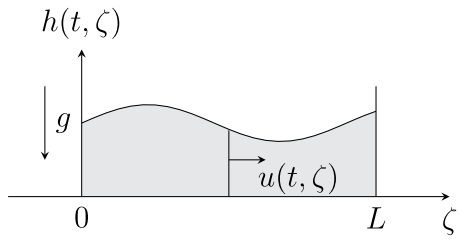

Fig. 1. The one-dimensional shallow water equation.

the normal and tangential projections on $\partial\Omega$ of the co-energy variables $\boldsymbol{e} := \delta_{\boldsymbol{x}}\mathcal{H}$ and dissipative effort $\boldsymbol{e}_d$, such that:

$$\dot{\mathcal{H}} = \int_{\partial\Omega} \boldsymbol{f}_\partial \cdot \boldsymbol{e}_\partial \,\mathrm{d}\gamma - \int_{\Omega} \boldsymbol{f}_d \cdot \boldsymbol{e}_d \,\mathrm{d}\,\Omega \leq \int_{\partial\Omega} \boldsymbol{f}_\partial \cdot \boldsymbol{e}_\partial \,\mathrm{d}\gamma, \tag{7}$$

where $\int_{\partial\Omega} \boldsymbol{f}_\partial \cdot \boldsymbol{e}_\partial \,\mathrm{d}\gamma$ describes the power supplied to the system through the boundaries and $\int_{\Omega} \boldsymbol{f}_d \cdot \boldsymbol{e}_d \,\mathrm{d}\,\Omega$ the power dissipated into heat by the internal phenomena (such as friction or viscosity).

2.3. Example of shallow water equations

The SWE are among the most researched fluid dynamical problems within the pH framework. These non-linear, wave-like equations have found applications in various domains. They have been employed, for example, to model free-surface fluids in water channels (see, for instance, [68,69,109]), as well as for simulating and controlling fluids in moving tanks and fluid–structure systems (see [32,33]).

In this subsection, we aim to provide a clear and pedagogical exposition of the 1D SWE within the context of the pH framework, which can be found in Section 2.3.1. Subsequently, we extend our discussion to the 2D version of these equations, presented in Section 2.3.2.

2.3.1. 1D SWE

The 1D SWE are nonlinear PDEs, typically written as two conservation laws, the first one models the conservation of mass, while the second one model the conservation of linear momentum:

$$\begin{cases} \partial_t h = -\partial_\zeta (hu) \,, \\ \partial_t u = -\partial_\zeta \left(\dfrac{u^2}{2} + gh \right) \,, \end{cases} \tag{8}$$

where $h(\zeta, t)$ is the fluid height, $u(\zeta, t)$ the fluid average velocity in a cross-section, ζ the spatial coordinate, t the time and g the gravitational acceleration, see Fig. 1 for a schematic view of the different variables in play.

The total energy $\mathcal{T}$ of the system inside the 1D domain $\Omega = [0, L]$ is given by the sum of kinetic and potential (gravitational) energy:

$$\mathcal{T} = \frac{1}{2} \int_{[0,L]} \left(\rho b\, hu^2 + \rho b g\, h^2 \right) \mathrm{d}\,\zeta \,, \tag{9}$$

where b is the width of the water channel (or fluid tank) and ρ the fluid density (assumed to be a constant). Defining the energy variables $q(\zeta, t) := bh(\zeta, t)$ and $\alpha(\zeta, t) := \rho u(\zeta, t)$, the system Hamiltonian (total energy) is given by:

$$\mathcal{H}\left[q(\zeta, t), \alpha(\zeta, t)\right] = \frac{1}{2} \int_{[0,L]} \left(\frac{q\alpha^2}{\rho} + \frac{\rho g}{b} q^2 \right) \mathrm{d}\,\zeta \,. \tag{10}$$

Using these newly defined variables, (8) can be rewritten as[4]:

$$\begin{pmatrix} \partial_t q \\ \partial_t \alpha \end{pmatrix} = \underbrace{\begin{pmatrix} 0 & -\partial_\zeta \\ -\partial_\zeta & 0 \end{pmatrix}}_{\mathcal{J}} \begin{pmatrix} e_q \\ e_\alpha \end{pmatrix}, \tag{11}$$

[4] In this case, $\mathcal{J} : H^1(\Omega)\times H^1(\Omega) \subset L^2(\Omega)\times L^2(\Omega) \to L^2(\Omega)\times L^2(\Omega)$ is indeed formally skew-symmetric, thanks to integration by parts, see Appendix A

where $e_q(\zeta, t)$ and $e_\alpha(\zeta, t)$ are the co-energy variables (respectively, the total pressure and the water flow) which are defined as the variational derivatives of the Hamiltonian with respect to $q(\zeta, t)$ and $\alpha(\zeta, t)$:

$$\begin{cases} e_q := \dfrac{\delta \mathcal{H}}{\delta q} = \dfrac{\alpha^2}{2\rho} + \dfrac{\rho g}{b} q = \rho \left(\dfrac{u^2}{2} + gh \right) \,, \\ e_\alpha := \dfrac{\delta \mathcal{H}}{\delta \alpha} = \dfrac{q\alpha}{\rho} = bhu \,. \end{cases} \tag{12}$$

Finally, from the time-derivative of the Hamiltonian (10) along the trajectories constrained to (11), one obtains the following power balance:

$$\begin{aligned} \dot{\mathcal{H}} &= \int_{[0,L]} \left(e_q(\zeta, t)\dot{q}(\zeta, t) + e_\alpha(\zeta, t)\dot{\alpha}(\zeta, t) \right) \mathrm{d}\,\zeta \,, \\ &= -\int_{[0,L]} \frac{\partial}{\partial \zeta} \left(e_q(\zeta, t) e_\alpha(\zeta, t) \right) \mathrm{d}\,\zeta \,, \\ &= -\int_{\partial[0,L]} e_q(\zeta, t) e_\alpha(\zeta, t) \mathrm{d}\,\zeta \,, \\ &= \boldsymbol{e}_\partial^T \boldsymbol{f}_\partial \,, \end{aligned} \tag{13}$$

where the effort boundary ports, $\boldsymbol{e}_\partial$, are defined as the values of the co-energy variable e_α evaluated in the spatial domain boundary:

$$\boldsymbol{e}_\partial := \begin{pmatrix} e_\alpha(0, t) \\ e_\alpha(L, t) \end{pmatrix} \,, \tag{14}$$

while the power-conjugate flow boundary ports $\boldsymbol{f}_\partial$ are defined as:

$$\boldsymbol{f}_\partial := \begin{pmatrix} e_q(0, t) \\ -e_q(L, t) \end{pmatrix} \,. \tag{15}$$

Remark 1. Eqs. (11), together with the Hamiltonian (10) and the co-energy variables (12) and boundary effort/flow (14), (15) definitions, describe a distributed-parameter pH system as presented in Definition 1, with $\boldsymbol{x} := \begin{pmatrix} q \\ \alpha \end{pmatrix}$ as state.

Furthermore, one may identify the distributed flow $\boldsymbol{f} := \begin{pmatrix} \partial_t q \\ \partial_t \alpha \end{pmatrix}$ and effort $\boldsymbol{e} := \begin{pmatrix} e_q \\ e_\alpha \end{pmatrix}$ variables, together with the boundary ports $\boldsymbol{f}_\partial$ and $\boldsymbol{e}_\partial$. They belong to a Dirac structure $\mathcal{D}$, *i.e.* $(\boldsymbol{f}, \boldsymbol{e}, \boldsymbol{f}_\partial, \boldsymbol{e}_\partial) \in \mathcal{D}$ at any time $t > 0$, which is generated by the structure operator $\mathcal{J}$ and the boundary variables.

Remark 2. The effort/flow boundary ports, defined in (14) and (15) represent one possible choice of boundary ports as defined in the general setting (3). The choices made here exhibit a clear physical meaning: they represent the fluid total pressure and volumetric flow at the boundaries (such that their product represents the power that flows through the boundary). Obviously, only one of these ports can be imposed at a given time. Typically, from a control perspective, these variables are written as input and output (observation) variables (since one of them is imposed as a control input, and the other is an output).

Remark 3. It is possible to modify (11) to introduce a distributed dissipation function. The friction of the fluid with the channel bottom is usually introduced as a force e_d distributed along the fluid:

$$\underbrace{\begin{pmatrix} \partial_t q \\ \partial_t \alpha \end{pmatrix}}_{\partial_t \boldsymbol{x}} = \underbrace{\begin{pmatrix} 0 & -\partial_\zeta \\ -\partial_\zeta & 0 \end{pmatrix}}_{\mathcal{J}} \underbrace{\begin{pmatrix} e_q \\ e_\alpha \end{pmatrix}}_{\boldsymbol{e}} + \begin{pmatrix} 0 \\ e_d \end{pmatrix}, \tag{16}$$

where e_d is proportional and opposite to the fluid momentum, *i.e.* $e_d = -Se_\alpha$. Thus, defining $f_d := -e_\alpha$, we can recast this dissipative version of the SWE as:

$$\begin{pmatrix} \partial_t \boldsymbol{x}(\zeta, t) \\ f_d \end{pmatrix} = \underbrace{\begin{bmatrix} \mathcal{J} & 1 \\ -1 & 0 \end{bmatrix}}_{\tilde{\mathcal{J}}} \begin{pmatrix} \boldsymbol{e} \\ e_d \end{pmatrix}, \text{ with } e_d = S f_d \,. \tag{17}$$

It is straightforward to verify that the power balance is given by:

$$\begin{aligned}\dot{\mathcal{H}} &= -\int_{[0,L]} f_d e_d \,\mathrm{d}\zeta + \boldsymbol{e}_\partial^T \boldsymbol{f}_\partial\,,\\ &= -\int_{[0,L]} S f_d{}^2 \,\mathrm{d}\zeta + \boldsymbol{e}_\partial^T \boldsymbol{f}_\partial \le \boldsymbol{e}_\partial^T \boldsymbol{f}_\partial\,.\end{aligned} \tag{18}$$

Consequently, the Eqs. (17) together with the system Hamiltonian and boundary ports, define a distributed-parameter dissipative pH system as presented in Definition 2.

The definition of S, which can be a nonlinear function of the energy variables q and α, such as $S = S(q,\alpha) \ge 0$ lead to different water-bed friction models that are commonly found in the SWE literature. For instance, the Darcy–Weisbach model is such that $S = \frac{f_{DW}\, b|\alpha|}{8q}$, where f_{DW} is an empirically obtained friction coefficient (see, for instance, [81, Sec. 7.2.6]).

In addition, a dissipation model related to fluid viscosity can also be obtained, as we recently presented in [29].

2.3.2. 2D SWE

Similarly, in a 2D setting, the frictionless SWE can be written as[5]:

$$\begin{pmatrix}\partial_t h\\ \partial_t \boldsymbol{\alpha}\end{pmatrix} = \underbrace{\begin{bmatrix}0 & -\mathrm{div}\\ -\mathbf{grad} & 0\end{bmatrix}}_{\mathcal{J}} \begin{pmatrix}e_h\\ \boldsymbol{e}_\alpha\end{pmatrix}, \tag{19}$$

where $h(\boldsymbol{\zeta},t)$ is the height of the fluid, $\boldsymbol{\alpha}(\boldsymbol{\zeta},t) := \rho\boldsymbol{u}$ is the linear momentum, $e_h = \frac{1}{2}\rho\|\boldsymbol{u}\|^2 + \rho g h$ is the total pressure, $\boldsymbol{e}_\alpha = h\boldsymbol{u}$ is the volumetric flow of the fluid and $\boldsymbol{\zeta}$ is the spatial coordinate variable.

The total energy $\mathcal{T}$ of the fluid is given by:

$$\mathcal{T} = \int_\Omega \frac{1}{2}\rho h\|\boldsymbol{u}\|^2 + \frac{1}{2}\rho g h^2 \,\mathrm{d}\Omega\,, \tag{20}$$

Rewriting as a functional of the energy variables h and $\boldsymbol{\alpha}$, we can define the system Hamiltonian:

$$\mathcal{H}[h(\boldsymbol{\zeta},t),\boldsymbol{\alpha}(\boldsymbol{\zeta},t)] := \int_\Omega \frac{1}{2\rho} h\|\boldsymbol{\alpha}\|^2 + \frac{1}{2}\rho g h^2 \,\mathrm{d}\Omega\,. \tag{21}$$

The co-energy variables are given by the variational derivative of the Hamiltonian:

$$\begin{aligned} e_h &:= \delta_h \mathcal{H} = \frac{1}{2\rho}\|\boldsymbol{\alpha}\|^2 + \rho g h = \frac{1}{2}\rho\|\boldsymbol{u}\|^2 + \rho g h\,,\\ \boldsymbol{e}_\alpha &:= \delta_{\boldsymbol{\alpha}} \mathcal{H} = h\frac{\boldsymbol{\alpha}}{\rho} = h\boldsymbol{u}\,.\end{aligned} \tag{22}$$

The power-balance of the system can then be computed from the time-derivative of the Hamiltonian as:

$$\dot{\mathcal{H}} = \int_\Omega \left(\partial_t h\, e_h + \partial_t \boldsymbol{\alpha}\cdot\boldsymbol{e}_\alpha\right)\mathrm{d}\Omega\,. \tag{23}$$

Then, from (19), and using Stokes theorem[6]:

$$\dot{\mathcal{H}} = \int_{\partial\Omega} e_h \left(-\boldsymbol{e}_\alpha\cdot\boldsymbol{n}\right)\mathrm{d}\gamma\,, \tag{24}$$

which enables to define collocated flow and effort distributed ports along the boundary $\partial\Omega$. For example:

$$\begin{aligned} e_\partial &= -\boldsymbol{e}_\alpha\cdot\boldsymbol{n}\,,\\ f_\partial &= e_h\,,\end{aligned} \tag{25}$$

and the power-balance is given by a product between the flow and effort boundary ports:

$$\dot{\mathcal{H}} = \int_{\partial\Omega} e_\partial f_\partial \,\mathrm{d}\gamma\,. \tag{26}$$

Remark 4. The Eqs. (19), together with the definitions of the system Hamiltonian, the co-energy variables and the boundary ports define a distributed-parameter pH system, as presented in Definition 1.

Remark 5. A modified version of (19) can be defined, that takes into account the (scalar) vorticity $\omega := \mathrm{curl}_{2D}\boldsymbol{u} = \partial_{\zeta_1}u_2 - \partial_{\zeta_2}u_1$ of the fluid:

$$\begin{pmatrix}\partial_t h\\ \partial_t \boldsymbol{\alpha}\end{pmatrix} = \begin{bmatrix}0 & -\mathrm{div}\\ -\mathbf{grad} & h^{-1}.G(\omega)\end{bmatrix}\begin{pmatrix}e_h\\ \boldsymbol{e}_\alpha\end{pmatrix}, \tag{27}$$

where $G(\omega) := \rho\begin{bmatrix}0 & 1\\ -1 & 0\end{bmatrix}\omega$. Since the matrix $G(\omega)$ is skew-symmetric, it will play no role in the power balance (and it computes exactly as (26)).

2.4. Example of incompressible Navier–Stokes equations

The NSE for a Newtonian fluid filling a domain $\Omega \subset \mathbb{R}^n$, $n = 2,3$, commonly read [16,35]:

$$\begin{cases}\partial_t \rho + \mathrm{div}(\rho\,\boldsymbol{u}) = 0\,,\\ \rho\,(\partial_t + \boldsymbol{u}\cdot\mathbf{grad})\boldsymbol{u} = -\mathbf{grad}(P) + \mu\,\boldsymbol{\Delta}\boldsymbol{u} + (\lambda+\mu)\,\mathbf{grad}(\mathrm{div}(\boldsymbol{u}))\,,\end{cases} \tag{28}$$

where ρ is the mass density, $\boldsymbol{u}$ is the particle velocity, P is the static pressure, $\mu > 0$ is the dynamic viscosity, and λ is related to $\eta := \lambda + \frac{2}{3}\mu$, known as the bulk viscosity, the latter being equal to 0 under Stokes assumption (in which case, $\lambda = -\frac{2}{3}\mu$).

Thanks to the identity $-\boldsymbol{\Delta} = \mathbf{curl}\,\mathbf{curl} - \mathbf{grad}\,\mathrm{div}$, the linear momentum evolution rewrites:

$$\rho\,\partial_t\boldsymbol{u} = -\rho\,(\boldsymbol{u}\cdot\mathbf{grad})\boldsymbol{u} - \mathbf{grad}(P) - \mu\,\mathbf{curl}(\mathbf{curl}(\boldsymbol{u})) + (\lambda+2\mu)\,\mathbf{grad}(\mathrm{div}(\boldsymbol{u}))\,.$$

Let $\rho \mapsto e(\rho)$ be the internal energy density, and define the Hamiltonian functional as the total energy of the system:

$$\mathcal{E} := \int_\Omega \left(\frac{1}{2}\rho\|\boldsymbol{u}\|^2 + \rho\, e(\rho)\right)\mathrm{d}\Omega.$$

Choosing the density ρ and the velocity $\boldsymbol{u}$ as energy variables, one can compute the co-energy variables $e_\rho := \delta_\rho\mathcal{E} = \frac{1}{2}\|\boldsymbol{u}\|^2 + \frac{P}{\rho} = h(\rho,\boldsymbol{u})$ which is the *enthalpy* density, and $\boldsymbol{e}_{\boldsymbol{u}} := \delta_{\boldsymbol{u}}\mathcal{E} = \rho\boldsymbol{u}$ which is the linear momentum density.

Let us introduce two extra dissipation ports:

- $\boldsymbol{f}_c := \boldsymbol{\omega} = \mathbf{curl}\,\boldsymbol{u} = \mathbf{curl}(\rho^{-1}\boldsymbol{e}_{\boldsymbol{u}})$,
- $f_d := \mathrm{div}\,\boldsymbol{u} = \mathrm{div}(\rho^{-1}\boldsymbol{e}_{\boldsymbol{u}})$,

which are both physically meaningful, and add the *closure relations* $e_d = \mu_d f_d$ and $\boldsymbol{e}_c = \mu_c \boldsymbol{f}_c$ (with $\mu_c = \mu$ and $\mu_d = \lambda + 2\mu = \frac{4}{3}\mu$). Then, following [96], we are in a position to recast the NSE for an isentropic Newtonian fluid as a pH system.

Theorem 1. *The NSE (28) rewrites:*

$$\begin{pmatrix}\partial_t\rho\\ \partial_t\boldsymbol{u}\\ \boldsymbol{f}_c\\ f_d\end{pmatrix} = \widetilde{\mathcal{J}}\begin{pmatrix}e_\rho\\ \boldsymbol{e}_{\boldsymbol{u}}\\ \boldsymbol{e}_c\\ e_d\end{pmatrix}, \tag{29}$$

where the interconnection differential operator $\widetilde{\mathcal{J}}$ is:

$$\widetilde{\mathcal{J}} = \begin{bmatrix}0 & -\mathrm{div} & 0 & 0\\ -\mathbf{grad} & \rho^{-1}.G(\boldsymbol{\omega}) & -\rho^{-1}.\mathbf{curl} & \rho^{-1}.\mathbf{grad}\\ 0 & \mathbf{curl}(\rho^{-1}.) & 0 & 0\\ 0 & \mathrm{div}(\rho^{-1}.) & 0 & 0\end{bmatrix}. \tag{30}$$

[5] The structure operator $\mathcal{J} : H^1(\Omega)\times H^{\mathrm{div}}(\Omega) \subset L^2(\Omega)\times(L^2(\Omega))^2 \to L^2(\Omega)\times(L^2(\Omega))^2$ is well-defined and formally skew-symmetric thanks to Green's formula, see Appendix A

[6] The power flow through the boundary is a duality bracket between $H^{\frac{1}{2}}(\partial\Omega)$, $H^{-\frac{1}{2}}(\partial\Omega)$ in general. However, we assume strong solution in this work (see Remark 19), reducing this bracket to a more convenient L^2-inner product at the boundary. More involved discussions and results about this concern may be found in *e.g.* [67, Section 2.1] or [30, Section 3.1] and the many references therein.

Defining as state variable $\boldsymbol{x} := \begin{pmatrix}\rho & \boldsymbol{u}^\top\end{pmatrix}^\top$, *collecting the dissipative variables into vectors* $\boldsymbol{e}_d := \begin{pmatrix}\boldsymbol{e}_c^\top & e_d\end{pmatrix}^\top$ *and* $\boldsymbol{f}_d := \begin{pmatrix}\boldsymbol{f}_c^\top & f_d\end{pmatrix}^\top$ *related by the closure relation* $\boldsymbol{e}_d = S\boldsymbol{f}_d$, *with* $S = Diag(\mu_c I_n, \mu_d)$, *gives a dissipative pH system in the sense of Definition 2, provided appropriate collocated boundary controls and observations are added.*

Proof. See [96, eq. (22)]. □

Let us now consider an incompressible fluid with constant mass density $\rho \equiv \rho_0$. The first line of (29) simplifies, and multiplying the second line by ρ_0 leads to:

$$\begin{pmatrix}\rho_0\partial_t\boldsymbol{u}\\ \boldsymbol{f}_c\\ 0\end{pmatrix} = \begin{bmatrix}G(\boldsymbol{\omega}) & -\mathbf{curl} & \mathbf{grad}\\ \mathbf{curl} & 0 & 0\\ \mathrm{div} & 0 & 0\end{bmatrix}\begin{pmatrix}\boldsymbol{u}\\ \boldsymbol{e}_c\\ e_d\end{pmatrix}. \tag{31}$$

The divergence-free constraint $f_d = \mathrm{div}(\boldsymbol{u}) = 0$ is ensured by the presence of a Lagrange multiplier in the dynamics, under the form $\mathbf{grad}(e_d)$, where $-e_d = P + \frac{1}{2}\rho_0\|\boldsymbol{u}\|^2$ is the total pressure. Hence, the pressure is determined up to a constant in these equations, as expected for incompressible fluids. It is intrinsically an infinite-dimensional pH-DAE. The linearized Navier–Stokes model at low Reynolds number, known as Oseen PDE, deserves a specific study; the Oseen model recast in a pH setting has recently been tackled in [120]. For the reformulation of the Navier–Stokes system and the removal of the pressure term, see e.g. [47,128], where an explicit solution formula for the linear case is provided.

Theorem 2. *The kinetic energy* $\mathcal{H} = \frac{1}{2}\int_\Omega \rho_0\|\boldsymbol{u}\|^2$ *satisfies the power-balance:*

$$\begin{aligned}\dot{\mathcal{H}} &= -\int_\Omega \boldsymbol{e}_c\cdot\boldsymbol{f}_c + \int_{\partial\Omega}\left(e_d\,\boldsymbol{u}\cdot\boldsymbol{n} - \boldsymbol{e}_c\cdot(\boldsymbol{u}\wedge\boldsymbol{n})\right),\\ &= -\int_\Omega \mu_c\|\boldsymbol{\omega}\|^2 + \int_{\partial\Omega}\left(\left(P+\frac{1}{2}\rho_0\|\boldsymbol{u}\|^2\right)\boldsymbol{u}\cdot\boldsymbol{n} - \mu_c\,\boldsymbol{\omega}\cdot(\boldsymbol{u}\wedge\boldsymbol{n})\right).\end{aligned} \tag{32}$$

Proof. See Appendix B.1. □

Remark 6. The negative term in (32) represents the transfer of kinetic energy into internal energy due to the viscosity.

Remark 7. The boundary power flows show that the normal velocity $\boldsymbol{u}\cdot\boldsymbol{n}$ is available for boundary control, whether the fluid be viscous or not, while the viscous damping is mandatory to have access to the tangential control of the velocity $\boldsymbol{u}\wedge\boldsymbol{n}$, since it is multiplied by the viscous term μ_c.

From now on, we only consider the 2D case. Our goal is to rewrite the initial problem given in a velocity–pressure formulation into an equivalent problem written in vorticity-stream function, see *e.g.* [84]. Following [35, §. 1.2], we recall that the curl_{2D} differential operator is defined by $\mathrm{curl}_{2D}(\boldsymbol{v}) := \partial_{\zeta_1}v_2 - \partial_{\zeta_2}v_1$, and that the following integration by parts formula holds:

$$\int_\Omega \mathrm{curl}_{2D}(\boldsymbol{v})\,w\,\mathrm{d}\Omega = \int_\Omega \boldsymbol{v}\cdot\mathbf{grad}^\perp(w)\,\mathrm{d}\Omega + \int_{\partial\Omega}(\Theta\boldsymbol{v})\cdot\boldsymbol{n}\;w\;\mathrm{d}\gamma, \tag{33}$$

where[7] $\mathbf{grad}^\perp(w) := \begin{pmatrix}\partial_{\zeta_2}w\\ -\partial_{\zeta_1}w\end{pmatrix}$, and Θ denotes the rotation of angle $-\frac{\pi}{2}$ in the 2D plane.

Applying curl_{2D} to the linear momentum conservation equation, the first line of (31), leads to the following evolution equation for the scalar vorticity $\omega := \mathrm{curl}_{2D}(\boldsymbol{u})$:

$$\rho_0\,\partial_t\omega = \mathrm{curl}_{2D}\left(G(\omega)\,\boldsymbol{u}\right) - \mu_c\,\mathrm{curl}_{2D}\,\mathbf{grad}^\perp(\omega),$$

where we have used $\boldsymbol{e}_c = \mu_c\,\mathbf{curl}\,\boldsymbol{u} = \mu_c\,\omega\,\boldsymbol{k}$ in 3D, and then $\mathbf{curl}(\omega\,\boldsymbol{k}) = \mathbf{grad}^\perp(\omega)$ in 2D (since the third component is 0). Another key point is that $\mathrm{curl}_{2D}\mathbf{grad} \equiv 0$. This classical trick enables eliminating the total pressure e_d from the system, as a Leray projector would do.

Assume moreover that the velocity $\boldsymbol{u}$ is fully determined by a stream function ψ, which is the case for instance if Ω is simply connected[8]; thus there exists a potential such that $\boldsymbol{u} = \mathbf{grad}^\perp\psi := \begin{pmatrix}\partial_{\zeta_2}\psi\\ -\partial_{\zeta_1}\psi\end{pmatrix}$. Substituting $\boldsymbol{u}$ with this definition gives in turn:

$$\rho_0\,\partial_t\omega = \mathrm{curl}_{2D}\left(G(\omega)\,\mathbf{grad}^\perp(\psi)\right) - \mu_c\,\mathrm{curl}_{2D}\,\mathbf{grad}^\perp(\omega). \tag{34}$$

Proposition 3. *For all sufficiently smooth functions* ψ:

$$\begin{aligned}&\mathrm{curl}_{2D}\left(G(\omega)\,\mathbf{grad}^\perp(\psi)\right) = \partial_{\zeta_1}(\omega\partial_{\zeta_2}\psi) - \partial_{\zeta_2}(\omega\partial_{\zeta_1}\psi),\\ &= \mathrm{div}\left(\omega\,\mathbf{grad}^\perp(\psi)\right),\\ &\qquad\qquad =: \quad J_\omega\psi.\end{aligned}$$

Furthermore, the operator J_ω, *which is modulated by the energy variable* ω, *is formally skew-symmetric, and satisfies Jacobi identities (see e.g. [106, Example 7.10]).*

Proof. Let us compute:

$$G(\omega)\,\mathbf{grad}^\perp(\psi) = \begin{pmatrix}0\\0\\\omega\end{pmatrix}\wedge\begin{pmatrix}\partial_{\zeta_2}\psi\\ -\partial_{\zeta_1}\psi\\0\end{pmatrix} = \begin{pmatrix}\omega\partial_{\zeta_1}\psi\\ \omega\partial_{\zeta_2}\psi\end{pmatrix} = \omega\,\mathbf{grad}\,\psi.$$

Applying curl_{2D} gives the claimed result.

Then, the formal skew-symmetry is obvious by integration by parts since, for all $\psi \in C_c^\infty(\Omega)$:

$$\int_\Omega \mathrm{div}\left(\omega\,\mathbf{grad}^\perp(\psi)\right)\psi\,\mathrm{d}\Omega = -\int_\Omega \omega\,\underbrace{\mathbf{grad}^\perp(\psi)\cdot\mathbf{grad}(\psi)}_{=0}\,\mathrm{d}\Omega.$$ □

The evolution equation (34) that replaces the initial linear momentum evolution, this induces a change in the energy variable that has to be considered to write the pH system. More precisely, the Hamiltonian $\mathcal{H}$ must now be considered as a functional of the vorticity:

$$\mathcal{H}(\omega) = \frac{1}{2}\int_\Omega \rho_0\|\boldsymbol{u}\|^2\,\mathrm{d}\Omega. \tag{35}$$

In turn, the co-energy variable has to be computed with respect to this new energy variable.

Proposition 4. *The variational derivative* $\delta_\omega\mathcal{H}(\omega)$ *of* $\mathcal{H}$ *is* $\rho_0\psi$.

Proof. This can be found in [106, Example 7.10] up to the presence of ρ_0, which plays no role in the computation. □

It is clear that the presence of ρ_0 has to be taken carefully into account. There are several ways to deal with it, but one elegant one is to include this (constant-in-time) parameter in the metric, leading to the following.

Corollary 5. *Consider the weighted* L^2*-inner product* $\langle u,v\rangle_{\rho_0} := \int_\Omega uv\rho_0\,\mathrm{d}\Omega$, *then the variational derivative of* $\mathcal{H}$, $e_\omega := \delta_\omega^{\rho_0}\mathcal{H}(\omega)$, *is* ψ.

Thanks to these results, one can finally write the dynamical system (34) in the pH form:

$$\begin{pmatrix}\rho_0\partial_t\omega\\ f_c\end{pmatrix} = \begin{bmatrix}J_\omega & -\mathrm{curl}_{2D}\mathbf{grad}^\perp\\ \mathrm{curl}_{2D}\mathbf{grad}^\perp & 0\end{bmatrix}\begin{pmatrix}\psi\\ e_c\end{pmatrix}, \tag{36}$$

with $\omega = \mathrm{curl}_{2D}\boldsymbol{u}$, $e_\omega = \psi$ and $e_c = \mu_c\omega$, together with the constitutive relation $e_c = \mu_c f_c$.

The power-balance (32) may be computed with respect to these new variables.

[7] Care must be taken that in some references, like [106] or [101], the opposite definition for $\mathbf{grad}^\perp$ is chosen. We stick to this one in order to be consistent with the formal adjoint of the curl_{2D} operator.

[8] In general, thanks to the Hodge–Helmholtz decomposition of $L^2(\Omega)$, the stream function is defined up to a divergence-free, irrotational potential.

Theorem 6. *The evolution of the Hamiltonian along the trajectories of dynamical system (36) with the closure relation is given by:*

$$\dot{\mathcal{H}} = -\int_\Omega \mu_c\,\omega^2 \mathrm{d}\,\Omega + \int_{\partial\Omega} \omega\,\psi\,\mathbf{grad}^\perp(\psi)\cdot\boldsymbol{n}\mathrm{d}\,\gamma + \mu_c\int_{\partial\Omega}(\psi\,\mathbf{grad}(\omega)\cdot\boldsymbol{n} - \omega\,\mathbf{grad}(\psi)\cdot\boldsymbol{n})\mathrm{d}\,\gamma\,, \tag{37}$$

where we can identify the tangential control $u_\tau = \mathbf{grad}(\psi)\cdot\boldsymbol{n}$ and the normal control $u_n = \mathbf{grad}^\perp(\psi)\cdot\boldsymbol{n}$.

Proof. See Appendix B.2 □

Remark 8. Note that both controls u_n and u_τ are available in this formulation. However, another term appears at the boundary in (37), namely $\mu_c\,\psi\,\mathbf{grad}(\omega)\cdot\boldsymbol{n}$, the physical meaning of which is not clear so far. Noticing that this can be viewed as the power flow corresponding to the boundary control of ψ, which obviously requires being compatible with both controls on $\boldsymbol{u}$, is crucial to successfully apply the PFEM, as will be enlightened in Section 3.

Nevertheless, a comparison of (37) with (32) allows deducing the following property about the pressure P:

Corollary 7.

$$\int_{\partial\Omega} P\,\mathbf{grad}^\perp(\psi)\cdot\boldsymbol{n}\mathrm{d}\,\gamma = \int_{\partial\Omega}\left(\left(\omega\,\psi - \frac{1}{2}\rho_0\|\mathbf{grad}^\perp(\psi)\|^2\right)\mathbf{grad}^\perp(\psi)\cdot\boldsymbol{n} + \mu_c\,\psi\,\mathbf{grad}(\omega)\cdot\boldsymbol{n}\right)\mathrm{d}\,\gamma.$$

Remark 9. In this context, the factorization of minus the 2D scalar Laplacian $-\Delta = \mathrm{curl}_{2D}\,\mathbf{grad}^\perp$ proves more appropriate than the usual one, namely $-\Delta = -\mathrm{div}\,\mathbf{grad}$. The computation is straightforward.

Remark 10. In (36), one can get rid of the realization of dissipation thanks to dissipative ports, and find the dissipative dynamics in the classical form $\mathcal{J} - \mathcal{G}\mathcal{S}\mathcal{G}^* = \mathcal{J} - \mathcal{R}$:

$$\rho_0\,\partial_t\omega = J_\omega\,\psi - \mu\,\Delta^2\psi\,, \quad \text{with} \quad \psi = \delta_\omega^{\rho_0}\mathcal{H}\,. \tag{38}$$

Moving from (36) to (38) is not only formal, indeed one of the two equivalent formulations can bring advantages in some applications: for example, the interest of the second formulation at the numerical level has been investigated in the case of the 2D dissipative shallow water equations in [29]. However, at the theoretical level, the first formulation with $\widetilde{\mathcal{J}}$ could be more beneficial, since the domains of the unbounded operators $\mathcal{J}_\omega$ and $\mathcal{R}$ could not coincide, and make the $(\mathcal{J}_\omega - \mathcal{R})$ formulation awkward, see e.g. [112] and references therein.

Remark 11. Now the 2D incompressible NSE depend wholly on 2 scalar fields, in comparison with the former velocity formulation which relied on one vector field and two scalar fields. At the discrete level, this considerably reduces the number of degrees of freedom.

3. Structure-preserving discretization

This section is devoted to the discretization of distributed pH systems in a structure-preserving way: the finite-dimensional discrete (in space) system must be a pH system, and its discrete Hamiltonian should satisfy a power balance that preserves the continuous power balance.

It is recalled in Appendix A that this power balance is encoded in a (Stokes-)Dirac structure [38], which can be represented as the graph of an extended structure operator constructed from the differential operator $\mathcal{J}$ and the boundary operators [22]. At the discrete level, it should result in two matrices M and J, the former being *symmetric*, and the latter *skew-symmetric*.

In addition to the discretization of the Stokes–Dirac structure, the constitutive relations require a particular attention to be consistent with the targeted discrete power balance.

The strategy adopted below relies on the mixed finite element method, well-established for elliptic problems, and known to be robust and efficient [15,59]. However, this approach does not allow capturing discontinuities as is, and would require further work.

3.1. Non-dissipative irrotational shallow water equations

Let us start with the Stokes–Dirac structure generated by the structure operator $\mathcal{J} = \begin{bmatrix} 0 & -\mathrm{div} \\ -\mathbf{grad} & 0 \end{bmatrix}$, *i.e.,* for the irrotational shallow water equation (19).

The weak formulation of (19) reads, for all test functions $(\varphi, \boldsymbol{\phi})$ smooth enough:

$$\begin{cases} \displaystyle\int_\Omega \partial_t h\varphi \mathrm{d}\,\Omega = -\int_\Omega \mathrm{div}\left(\boldsymbol{e}_\alpha\right)\varphi \mathrm{d}\,\Omega, \\ \displaystyle\int_\Omega \partial_t\boldsymbol{\alpha}\cdot\boldsymbol{\phi}\mathrm{d}\,\Omega = -\int_\Omega \mathbf{grad}\left(e_h\right)\cdot\boldsymbol{\phi}\mathrm{d}\,\Omega. \end{cases}$$

The boundary control $e_\partial = -\boldsymbol{e}_\alpha\cdot\boldsymbol{n}$, defined in (25), is taken into account by performing an integration by parts on the first line, leading to:

$$\begin{cases} \displaystyle\int_\Omega \partial_t h\varphi \mathrm{d}\,\Omega = \int_\Omega \boldsymbol{e}_\alpha\cdot\mathbf{grad}\left(\varphi\right)\mathrm{d}\,\Omega + \int_{\partial\Omega} e_\partial\varphi\mathrm{d}\,\gamma, \\ \displaystyle\int_\Omega \partial_t\boldsymbol{\alpha}\cdot\boldsymbol{\phi}\mathrm{d}\,\Omega = -\int_\Omega \mathbf{grad}\left(e_h\right)\cdot\boldsymbol{\phi}\mathrm{d}\,\Omega. \end{cases} \tag{39}$$

Consider three finite element families $(\varphi^i)_{i=1,\dots,N_h}$, $(\boldsymbol{\phi}^k)_{k=1,\dots,N_\alpha}$ and $(\xi^m)_{m=1,\dots,N_\partial}$ for the approximation of the h-type variables, the α-type variables and the boundary variables respectively, as follows:

$$h(\boldsymbol{\zeta},t) \simeq h^d(\boldsymbol{\zeta},t) := \sum_{i=1}^{N_h} h^i(t)\varphi^i(\boldsymbol{\zeta}), \quad e_h(\boldsymbol{\zeta},t) \simeq e_h^d(\boldsymbol{\zeta},t) := \sum_{i=1}^{N_h} e_h^i(t)\varphi^i(\boldsymbol{\zeta}),$$

for the scalar fields,

$$\boldsymbol{\alpha}(\boldsymbol{\zeta},t) \simeq \boldsymbol{\alpha}^d(\boldsymbol{\zeta},t) := \sum_{k=1}^{N_\alpha} \alpha^k(t)\boldsymbol{\phi}^k(\boldsymbol{\zeta}), \quad \boldsymbol{e}_{\boldsymbol{\alpha}}(\boldsymbol{\zeta},t) \simeq \boldsymbol{e}_{\boldsymbol{\alpha}}^d(\boldsymbol{\zeta},t) := \sum_{k=1}^{N_\alpha} e_\alpha^k(t)\boldsymbol{\phi}^k(\boldsymbol{\zeta}),$$

for the vector fields, and at the boundary:

$$e_\partial(\boldsymbol{s},t) \simeq e_\partial^d(\boldsymbol{s},t) := \sum_{m=1}^{N_\partial} e_\partial^m(t)\xi^m(\boldsymbol{s}), \quad f_\partial(\boldsymbol{s},t) \simeq f_\partial^d(\boldsymbol{s},t) := \sum_{m=1}^{N_\partial} f_\partial^m(t)\xi^m(\boldsymbol{s}).$$

The coefficients $\square^j(t)$ of the approximation $\square^d$ of $\square$ are collected in a vector denoted $\underline{\square}(t)$.

Plugging these approximations into (39) and taking the finite elements families as test functions, one gets:

$$\begin{bmatrix} M_h & 0 \\ 0 & M_{\boldsymbol{\alpha}} \end{bmatrix}\begin{pmatrix} \underline{\dot{h}}(t) \\ \underline{\dot{\alpha}}(t) \end{pmatrix} = \begin{bmatrix} 0 & D \\ -D^\top & 0 \end{bmatrix}\begin{pmatrix} \underline{e_h}(t) \\ \underline{e_\alpha}(t) \end{pmatrix} + \begin{bmatrix} B \\ 0 \end{bmatrix}\underline{e_\partial}(t), \tag{40}$$

where the mass matrices on the left-hand side are defined as:

$$(M_h)_{i,j} := \int_\Omega \varphi^j\,\varphi^i \mathrm{d}\,\Omega, \qquad (M_{\boldsymbol{\alpha}})_{k,\ell} := \int_\Omega \boldsymbol{\phi}^\ell\cdot\boldsymbol{\phi}^k \mathrm{d}\,\Omega,$$

and the differential and control matrices on the right-hand side are defined as:

$$(D)_{k,j} := \int_\Omega \boldsymbol{\phi}^k\cdot\mathbf{grad}\left(\varphi^j\right)\mathrm{d}\,\Omega, \qquad (B)_{m,j} := \int_{\partial\Omega}\xi^m\varphi^j\mathrm{d}\,\gamma.$$

Note that $D \in \mathbb{R}^{N_h\times N_\alpha}$ and $B \in \mathbb{R}^{N_h\times N_\partial}$ are not square matrices.

If furthermore one writes the weak form of the output f_∂ defined in (25), one obtains:

$$\int_{\partial\Omega} f_\partial\,\xi\mathrm{d}\,\gamma = \int_{\partial\Omega} e_h\,\xi\mathrm{d}\,\gamma,$$

which leads once approximated with the boundary finite elements:

$$M_\partial\underline{f_\partial}(t) = B^\top\underline{e_h}(t),$$

where the boundary mass matrix is defined as:

$$(M_\partial)_{m,\ell} := \int_{\partial\Omega} \xi^\ell \xi^m \mathrm{d}\gamma.$$

This latter equation gathered with (40) allows one to identify the matrices representing a finite-dimensional Dirac structure:

$$\underbrace{\begin{bmatrix} M_h & 0 & 0 \\ 0 & M_{\boldsymbol{\alpha}} & 0 \\ 0 & 0 & M_\partial \end{bmatrix}}_{\boldsymbol{M}} \begin{pmatrix} \dot{\underline{h}}(t) \\ \dot{\underline{\alpha}}(t) \\ -\underline{f_\partial}(t) \end{pmatrix} = \underbrace{\begin{bmatrix} 0 & D & B \\ -D^\top & 0 & 0 \\ -B^\top & 0 & 0 \end{bmatrix}}_{\boldsymbol{J}} \begin{pmatrix} \underline{e_h}(t) \\ \underline{e_\alpha}(t) \\ \underline{e_\partial}(t) \end{pmatrix}. \tag{41}$$

It is clear that $\boldsymbol{M}$ is symmetric positive-definite and that $\boldsymbol{J}$ is skew-symmetric. Then, the graph of $\boldsymbol{J}$ proves to be a Dirac structure in $\mathbb{R}^{(N_h+N_\alpha+N_\partial)^2}$ equipped with the metric induced by $\boldsymbol{M}$, see [133].

To achieve the structure-preserving discretization, it remains to take the constitutive relations into account, in such a way the power balance of the discrete Hamiltonian will mimic the continuous one.

At least two approaches may be used to reach our goal, which prove equivalent in the case of a polynomial (but not necessarily quadratic) Hamiltonian, as considered in this work. The first way is to define the constitutive relations at the discrete level, by making use of the gradient of the discrete Hamiltonian in the metrics induced by M_h and $M_{\boldsymbol{\alpha}}$, as it has been done, *e.g.,* in [31, Section 4.2]. On the other hand, one can directly write down the weak formulations of (22), as follows:

$$\int_\Omega e_h \varphi \mathrm{d}\Omega = \int_\Omega \|\boldsymbol{\alpha}\|^2 \frac{\varphi}{2\rho} \mathrm{d}\Omega + \int_\Omega h\, \rho g \varphi \mathrm{d}\Omega,$$
$$\int_\Omega \boldsymbol{e_\alpha} \cdot \boldsymbol{\phi} \mathrm{d}\Omega = \int_\Omega h\boldsymbol{\alpha} \cdot \frac{\boldsymbol{\phi}}{\rho} \mathrm{d}\Omega.$$

The finite element approximations then lead to:

$$M_h\, \underline{e_h}(t) = N[\underline{\alpha}(t)]\, \underline{\alpha}(t) + Q_h\, \underline{h}(t),$$

where:

$$(Q_h)_{i,j} := \int_\Omega \varphi^j \rho g \varphi^i \mathrm{d}\Omega, \qquad (N[\underline{\alpha}(t)])_{i,\ell} := \int_\Omega \frac{\boldsymbol{\alpha}^d}{2\rho} \cdot \boldsymbol{\phi}^\ell\, \varphi^i \mathrm{d}\Omega,$$

and,

$$M_{\boldsymbol{\alpha}}\, \underline{e_\alpha}(t) = Q_{\boldsymbol{\alpha}}[\underline{h}(t)]\, \underline{\alpha}(t),$$

where:

$$(Q_{\boldsymbol{\alpha}}[\underline{h}(t)])_{k,\ell} := \int_\Omega \frac{h^d}{\rho} \boldsymbol{\phi}^\ell \cdot \boldsymbol{\phi}^k \mathrm{d}\Omega.$$

These may be gathered in a more compact form as:

$$\begin{bmatrix} M_h & 0 \\ 0 & M_{\boldsymbol{\alpha}} \end{bmatrix} \begin{pmatrix} \underline{e_h}(t) \\ \underline{e_\alpha}(t) \end{pmatrix} = \begin{bmatrix} Q_h & N[\underline{\alpha}(t)] \\ 0 & Q_{\boldsymbol{\alpha}}[\underline{h}(t)] \end{bmatrix} \begin{pmatrix} \underline{h}(t) \\ \underline{\alpha}(t) \end{pmatrix}. \tag{42}$$

Let us define the discrete Hamiltonian $\mathcal{H}^d$ as the evaluation of the continuous one $\mathcal{H}$, defined in (21), in the approximated variables, as follows:

$$\mathcal{H}^d(\underline{h}(t), \underline{\alpha}(t)) := \mathcal{H}(h^d(t,\boldsymbol{x}), \boldsymbol{\alpha}^d(t,\boldsymbol{x})) = \int_\Omega \left[\frac{h^d}{2\rho} \left\|\boldsymbol{\alpha}^d\right\|^2 + \frac{\rho g}{2} (h^d)^2 \right] \mathrm{d}\Omega.$$

Hence, with the notations of this section, the discrete Hamiltonian $\mathcal{H}^d$ rewrites:

$$\mathcal{H}^d(\underline{h}(t), \underline{\alpha}(t)) = \frac{1}{2} \underline{\alpha}(t)^\top\, Q_{\boldsymbol{\alpha}}[\underline{h}(t)]\, \underline{\alpha}(t) + \frac{1}{2} \underline{h}(t)^\top\, Q_h\, \underline{h}(t). \tag{43}$$

Remark 12. As already said, the *polynomial* structure of the Hamiltonian is crucial in this work, as the discrete weak form of the variational derivatives of the continuous Hamiltonian turns out to be the gradient of the discrete Hamiltonian in the metric induced by the mass matrices. Indeed, compare (42) with [30, Eq. (4.25) and (4.29)]. This is indeed true, thanks to the equality:

$$\frac{1}{2} \underline{\alpha}(t)^\top\, Q_{\boldsymbol{\alpha}}[\underline{h}(t)]\, \underline{\alpha}(t) = \underline{\alpha}(t)^\top\, N[\underline{\alpha}(t)]^\top\, \underline{h}(t),$$

which would not occur if the Hamiltonian were not polynomial.

Thanks to this equality, the notations $Q_{\boldsymbol{\alpha}}[\underline{h}(t)]$ and $N[\underline{\alpha}(t)]$ indeed make sense, even if it is h^d and $\boldsymbol{\alpha}^d$, respectively, which appear in the definitions of the nonlinear matrices $Q_{\boldsymbol{\alpha}}[\underline{h}(t)]$ and $N[\underline{\alpha}(t)]$.

Two worked-out examples where the polynomial structure of the relations proves crucial in applying the PFEM can be found in [11] for Allen–Cahn model, and in [10] for the Cahn–Hilliard model.

Theorem 8. *Let $(\underline{h}(t), \underline{\alpha}(t), \underline{e_h}(t), \underline{e_\alpha}(t))$ be a trajectory, i.e., it satisfies the discrete system (41)–(42) for some initial data and some control $\underline{e_\partial}(t)$, for $t \geq 0$. Then, the discrete Hamiltonian $\mathcal{H}^d$ defined in (43) satisfies the discrete power balance:*

$$\frac{\mathrm{d}}{\mathrm{d}t} \mathcal{H}^d(\underline{h}(t), \underline{\alpha}(t)) = \underline{e_\partial}(t)^\top\, M_\partial \underline{f_\partial}(t), \tag{44}$$

which preserves the continuous one (26) at the discrete level.

Proof. See Appendix B.3 □

3.2. Tackling dissipation

Dissipation in the framework of pH systems has been presented in Section 2.2. It relies on an extra port $(\boldsymbol{f}_d, \boldsymbol{e}_d)$, called *dissipative*, which models the loss of energy (*i.e.,* the decay of $\mathcal{H}$). It has been recalled that such a port, combined with a dissipative constitutive relation linking $\boldsymbol{e}_d$ to $\boldsymbol{f}_d$ (*e.g.,* for linear dissipation $\boldsymbol{e}_d = S\boldsymbol{f}_d$ with $S > 0$), may be viewed as an appropriate decomposition of the dissipative operator $\mathcal{R} = \mathcal{G}S\mathcal{G}^\star$ of the PDE under consideration.

The PFEM is versatile enough to consider both approaches for simulations, either including $\mathcal{R}$ in the dynamics, or its decomposition $\mathcal{G}S\mathcal{G}^\star$. The former is straightforward as it does not need the addition of a dissipative port, while the latter may require more attention for discretization. The choice of one or the other form depends on the desired outcomes of the numerical experiments.

Nonlinear dissipation. In this case, $\mathcal{G} \equiv \begin{bmatrix} 0 \\ I \end{bmatrix}$ (the dissipation acts on the linear momentum equation) and the operator generating the nonlinear dissipation is considered outside the Dirac structure, *i.e.,* in the dissipative constitutive relation as $\mathcal{N}(h, \boldsymbol{\alpha}, \boldsymbol{e}_d, \boldsymbol{f}_d) = 0$, as presented for the 1D SWE in Remark 3. The dissipative port is of the same mathematical nature as the $\boldsymbol{\alpha}$-type port, and can be approximated with the same finite element family (although this is not mandatory). Hence, this leads to the extended Dirac structure:

$$\begin{bmatrix} M_h & 0 & 0 & 0 \\ 0 & M_{\boldsymbol{\alpha}} & 0 & 0 \\ 0 & 0 & M_{\boldsymbol{\alpha}} & 0 \\ 0 & 0 & 0 & M_\partial \end{bmatrix} \begin{pmatrix} \dot{\underline{h}}(t) \\ \dot{\underline{\alpha}}(t) \\ \underline{f_d}(t) \\ -\underline{f_\partial}(t) \end{pmatrix} = \begin{bmatrix} 0 & D & 0 & B \\ -D^\top & 0 & M_{\boldsymbol{\alpha}} & 0 \\ 0 & -M_{\boldsymbol{\alpha}} & 0 & 0 \\ -B^\top & 0 & 0 & 0 \end{bmatrix} \begin{pmatrix} \underline{e_h}(t) \\ \underline{e_\alpha}(t) \\ \underline{e_d}(t) \\ \underline{e_\partial}(t) \end{pmatrix}.$$

This Dirac structure implies straightforwardly the following power balance:

$$\frac{\mathrm{d}}{\mathrm{d}t} \mathcal{H}^d(\underline{h}(t), \underline{\alpha}(t)) = \underline{e_\partial}(t)^\top\, M_\partial \underline{f_\partial}(t) - \underline{e_d}(t)^\top\, M_{\boldsymbol{\alpha}}\, \underline{f_d}(t),$$

which contains the term $\underline{e_d}(t)^\top\, M_{\boldsymbol{\alpha}}\, \underline{f_d}(t)$, non-negative if the dissipative constitutive relation $\mathcal{N}(h, \boldsymbol{\alpha}, \boldsymbol{e}_d, \boldsymbol{f}_d) = 0$ is indeed a dissipation, *e.g.,* of the form $\boldsymbol{e}_d = C(\boldsymbol{\alpha}, h)\boldsymbol{f}_d$, with $C(\boldsymbol{\alpha}, h) \geq 0$. Such a constitutive relation would give at the discrete level: $M_{\boldsymbol{\alpha}}\, \underline{e_d} = C[h^d, \boldsymbol{\alpha}^d]\, \underline{f_d}$, with $C[h^d, \boldsymbol{\alpha}^d] \geq 0$. In this latter case, the power balance becomes:

$$\begin{aligned} \frac{\mathrm{d}}{\mathrm{d}t} \mathcal{H}^d(\underline{h}(t), \underline{\alpha}(t)) &= \underline{e_\partial}(t)^\top\, M_\partial \underline{f_\partial}(t) - \underline{f_d}(t)^\top C[h^d(t), \boldsymbol{\alpha}^d(t)]\, \underline{f_d}(t) \\ &\leq \underline{e_\partial}(t)^\top\, M_\partial \underline{f_\partial}(t). \end{aligned}$$

This encompasses the following empirical laws [81, § 7.2.6], which are used to model the friction of the fluid with the bottom of the channel:

- Fanning friction: $(C[h^d, \boldsymbol{\alpha}^d])_{k,\ell} = C_f \int_\Omega \frac{\|\boldsymbol{\alpha}^d\|}{h^d} \boldsymbol{\phi}^\ell \cdot \boldsymbol{\phi}^k \mathrm{d}\Omega$;

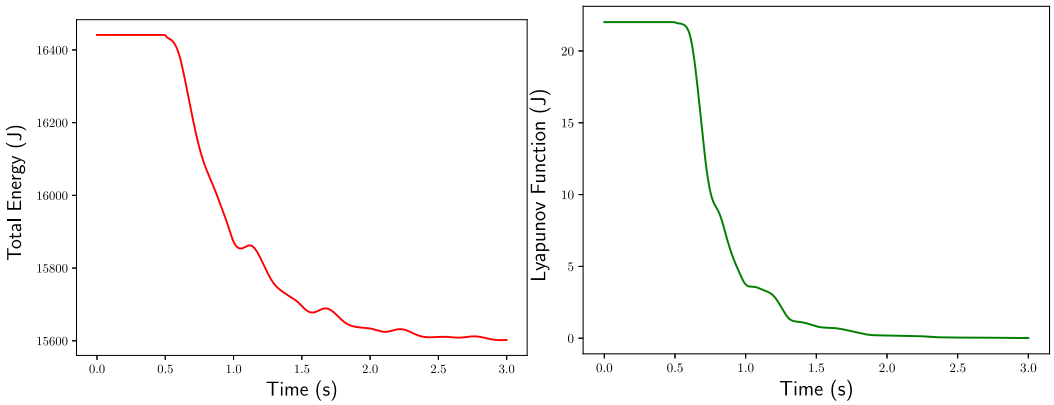

(a) Total energy (Hamiltonian) (b) Lyapunov function

Fig. 2. Total energy and Lyapunov Function.

- Manning friction: $(C[h^d, \boldsymbol{\alpha}^d])_{k,\ell} = gn^2 \int_\Omega \frac{\|\alpha^d\|}{(h^d)^{\frac{4}{3}}} \boldsymbol{\phi}^\ell \cdot \boldsymbol{\phi}^k \mathrm{d}\,\Omega$;
- Darcy–Weisbach: $(C[h^d, \boldsymbol{\alpha}^d])_{k,\ell} = \frac{f_{DW}}{8} \int_\Omega \frac{\|\alpha^d\|}{h^d} \boldsymbol{\phi}^\ell \cdot \boldsymbol{\phi}^k \mathrm{d}\,\Omega$;
- Kellerhals friction: $(C[h^d, \boldsymbol{\alpha}^d])_{k,\ell} = gr^2 \int_\Omega \frac{\|\alpha^d\|}{(h^d)^{\frac{3}{2}}} \boldsymbol{\phi}^\ell \cdot \boldsymbol{\phi}^k \mathrm{d}\,\Omega$.

Linear dissipation of Navier–Stokes type. Indeed, in addition to modeling the friction of the fluid with the bottom of the channel, viscous dissipation can be introduced by incorporating the analogue of the Navier–Stokes dissipative terms in the SWE model: it involves an unbounded linear operator. One could first guess to add a $-\boldsymbol{\Delta}$ diffusion term, as was first proposed in [31]; however the careful derivation of the damping model should be made with care, see [56] in 1D and [88] in 2D, where the model exhibits a h-dependent dissipation term. A structure-preserving pH discretization of this more advanced model, involving symmetric tensors, can be found in [29].

3.3. Example of the rotational SWE with boundary-feedback control

In this example, previously discussed in [28], a boundary-feedback control law is used with the goal of damping the waves. Indeed, one of the motivations for using the pH framework is that applying passivity-based control laws is straightforward. For example, a simple boundary output-feedback as:

$$f_\partial = -k e_\partial \,, \tag{45}$$

leads (26) to the following power-balance:

$$\frac{\mathrm{d}}{\mathrm{d}t}\mathcal{H} = -k \int_{\partial\Omega} \left(e_\partial\right)^2 \mathrm{d}\,\gamma \;, \tag{46}$$

from which the Hamiltonian is monotonically decreasing $\frac{\mathrm{d}}{\mathrm{d}t}\mathcal{H} \leq 0$ if $k > 0$. Recall that from (25), $e_\partial = -\boldsymbol{e}_\alpha \cdot \boldsymbol{n}$, is the ingoing volumetric fluid flux and $f_\partial = e_h$ is the pressure, both at the boundary.

This control law is of low applicability for the SWE, since it removes energy not only by damping the waves, but also by removing water from inside the tank (thus, the potential energy is reduced). For this reason, we used the following slightly modified control law:

$$f_\partial = -k(e_\partial - e_\partial^0) \,, \tag{47}$$

where e_∂^0 is the desired output, given by the steady-state total pressure at the boundary ($e_h = \rho g h^0$) at the desired fluid height h^0.

It is straightforward to prove that the previous boundary control law stabilizes the infinite-dimensional dynamical system in the sense of Lyapunov around an equilibrium: We can define a "desired Hamiltonian", or Lyapunov function, given by:

$$V = \int_\Omega \left[\frac{1}{2}\rho g \left(h - h^0\right)^2 + \frac{1}{2\rho} h \|\boldsymbol{\alpha}\|^2\right] \mathrm{d}\,\Omega \,, \tag{48}$$

By computing the time-derivative of the Lyapunov function along trajectories, using the feedback law proposed in (47), we get:

$$\dot{V} = -k \int_{\partial\Omega} \left(e_\partial - e_\partial^0(\theta)\right)^2 \mathrm{d}\,\gamma \,. \tag{49}$$

Thus, if $k > 0$, the Lyapunov function shall reduce monotonically towards the minimum point of (48) ($h = h^0$ and $\boldsymbol{\alpha} = \mathbf{0}$).

Numerical results for the closed-loop SWE

The feedback control law, from (47), can be implemented as an additional constitutive relationship that relates $\underline{f_\partial}$ and $\underline{e_\partial}$ in the finite-dimensional approximated system (41).

The following simulation considers a circular tank with radius R, with radial coordinate r and polar coordinate θ, assuming the following initial conditions:

$$\begin{aligned} &h(t=0, r, \theta) = \cos(\pi r/R)\cos(2\theta) \,, \\ &\boldsymbol{\alpha}(t=0, r, \theta) = \rho \boldsymbol{u} = \mathbf{0} \,. \end{aligned} \tag{50}$$

The boundary conditions are assumed to be:

$$\begin{aligned} &f_\partial = 0 \,, t \leq 0.5 \text{ s} \,, \\ &f_\partial = -k\left(e_\partial(t,s) - e_\partial^0\right) \,, t > 0.5 \text{ s} \,, \end{aligned} \tag{51}$$

i.e. the feedback control law proposed is activated after 0.5 s of simulation. A video of this simulation can be downloaded in https://nextcloud.isae.fr/index.php/s/4TrMBSZa86cL6w2.

Continuous Galerkin elements with 1st-order Lagrange polynomials are used for approximating the h variable, and discontinuous Galerkin elements with 0-order Lagrange polynomials are used for approximating the $\boldsymbol{\alpha}$ variables. The system Hamiltonian as well as the Lyapunov function are presented as a function of time in Fig. 2. Note that during the first 0.5 s of the simulation, both the Hamiltonian (total energy) and the Lyapunov function are constant. After 0.5 s, the Hamiltonian reduces and oscillates until converging to the new energy minimum. The Lyapunov function monotonically decreases towards zero. Snapshots of the simulation are presented in Fig. 3.

3.4. Example of the incompressible Navier–Stokes equations

In order to reduce as much as possible the number of degrees of freedom needed to discretize the incompressible NSE in a structure-preserving way, the vorticity–stream function formulation has been chosen in Section 2.4. However, some adaptations are required for the boundary controls to remain identical to those of the initial system, as another term appears in the power balance (37). Furthermore, the constitutive relation linking the vorticity ω to the stream function ψ reveals differential: $-\Delta\psi = \omega$. This means that at least two choices are possible for the resolution in time of the discrete system: either

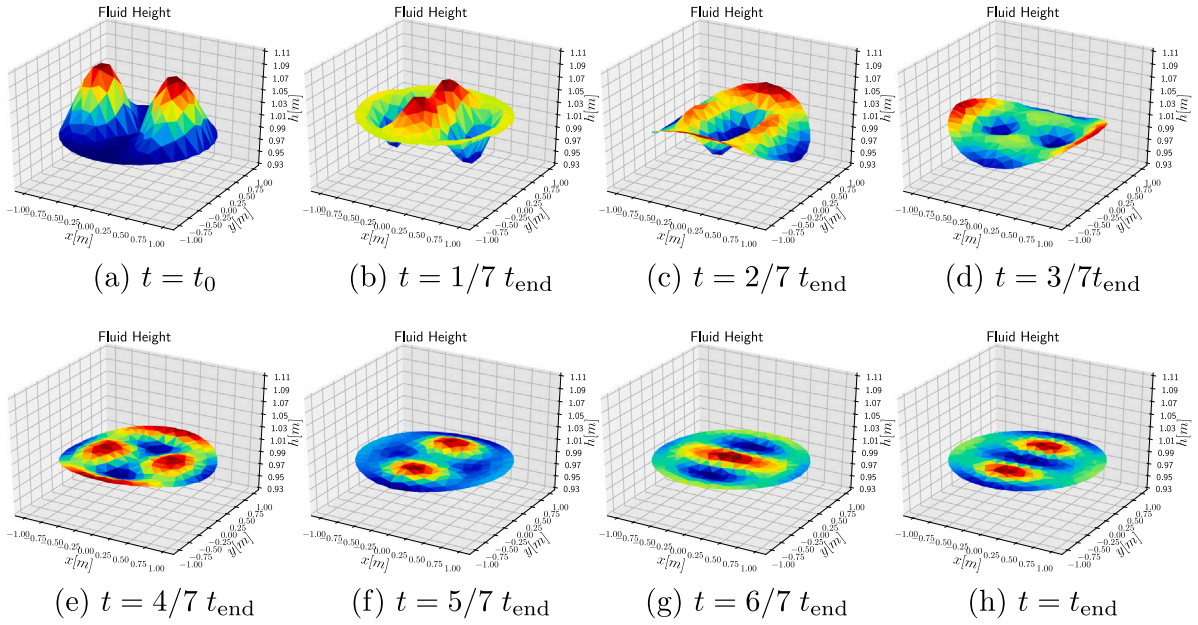

Fig. 3. Boundary control using a proportional gain $t_{\text{end}} = 3[s]$.

we differentiate twice, requiring sufficiently rich finite elements, or we perform an integration by part to reduce the order of derivation, to the price of another boundary term, involving the time derivative of the control. In the following, the latter is chosen, in an implicit form: the constitutive relation is embedded in the dynamical system, see (52).

Indeed, to reduce the complexity of the system, an efficient strategy is to consider the *co-energy formulation*, involving only the co-energy and effort variables by substituting the constitutive relations into the dynamical system: $-\Delta\psi = \omega$, and $\mu_c^{-1}\ e_c = f_c$ are used in (36), leading to the system:

$$\begin{pmatrix} -\rho_0\ \Delta\partial_t\psi \\ \mu_c^{-1}\ e_c \end{pmatrix} = \begin{bmatrix} J_\omega & -\text{curl}_{2D}\ \mathbf{grad}^\perp \\ \text{curl}_{2D}\ \mathbf{grad}^\perp & 0 \end{bmatrix} \begin{pmatrix} \psi \\ e_c \end{pmatrix}. \tag{52}$$

We may now apply the PFEM: we write the weak formulation of (52), perform appropriate integration by part, and project the system on finite element families.

For all sufficiently smooth test functions $(\varphi, \boldsymbol{\Phi})$, one has:

$$\begin{cases} -\displaystyle\int_\Omega \rho_0\ \partial_t\Delta\psi\ \varphi\,\mathrm{d}\,\Omega = \int_\Omega J_\omega\psi\ \varphi\,\mathrm{d}\,\Omega - \int_\Omega \text{curl}_{2D}\ \mathbf{grad}^\perp\left(e_c\right)\ \varphi\,\mathrm{d}\,\Omega, \\ \displaystyle\int_\Omega \mu_c^{-1}\ e_c\ \boldsymbol{\Phi}\,\mathrm{d}\,\Omega = \int_\Omega \text{curl}_{2D}\ \mathbf{grad}^\perp(\psi)\ \boldsymbol{\Phi}\,\mathrm{d}\,\Omega. \end{cases} \tag{53}$$

Every differential operators in this system, including J_ω, are of second order. Let us integrate by part on each of them.

$$\begin{aligned} &-\int_\Omega \rho_0\ \partial_t\Delta\psi\ \varphi\,\mathrm{d}\,\Omega = -\int_\Omega \rho_0\ \Delta\partial_t\psi\ \varphi\,\mathrm{d}\,\Omega \\ &= \int_\Omega \rho_0\ \mathbf{grad}\left(\partial_t\psi\right)\cdot\mathbf{grad}\left(\varphi\right)\,\mathrm{d}\,\Omega - \int_{\partial\Omega} \rho_0\ \mathbf{grad}\left(\partial_t\psi\right)\cdot\boldsymbol{n}\ \varphi\,\mathrm{d}\,\gamma \\ &= \int_\Omega \rho_0\ \mathbf{grad}\left(\partial_t\psi\right)\cdot\mathbf{grad}\left(\varphi\right)\,\mathrm{d}\,\Omega - \int_{\partial\Omega} \rho_0\ \partial_t \underbrace{\mathbf{grad}\left(\psi\right)\cdot\boldsymbol{n}}_{\boldsymbol{u}\wedge\boldsymbol{n}=u_\tau}\ \varphi\,\mathrm{d}\,\gamma. \end{aligned} \tag{54}$$

$$\begin{aligned} &\int_\Omega J_\omega\psi\ \varphi\,\mathrm{d}\,\Omega = \int_\Omega \text{div}\left(\omega\mathbf{grad}^\perp(\psi)\right)\ \varphi\,\mathrm{d}\,\Omega \\ &= -\int_\Omega \omega\,\mathbf{grad}^\perp(\psi)\cdot\mathbf{grad}\left(\varphi\right)\,\mathrm{d}\,\Omega \\ &\quad + \int_{\partial\Omega} \omega\ \underbrace{\mathbf{grad}^\perp(\psi)\cdot\boldsymbol{n}}_{\boldsymbol{u}\cdot\boldsymbol{n}=u_n}\ \varphi\,\mathrm{d}\,\gamma. \end{aligned} \tag{55}$$

$$\begin{aligned} -\int_\Omega \text{curl}_{2D}\ \mathbf{grad}^\perp\left(e_c\right)\ \varphi\,\mathrm{d}\,\Omega &= -\int_\Omega \mathbf{grad}^\perp\left(e_c\right)\cdot\mathbf{grad}^\perp\left(\varphi\right)\mathrm{d}\,\Omega \\ &\quad + \int_{\partial\Omega} \underbrace{\left(\mathbf{grad}\left(e_c\right)\right)\cdot\boldsymbol{n}}_{=y_c}\ \varphi\,\mathrm{d}\,\gamma. \end{aligned} \tag{56}$$

$$\begin{aligned} \int_\Omega \text{curl}_{2D}\ \mathbf{grad}^\perp(\psi)\ \boldsymbol{\Phi}\,\mathrm{d}\,\Omega &= \int_\Omega \mathbf{grad}^\perp(\psi)\cdot\mathbf{grad}^\perp(\boldsymbol{\Phi})\,\mathrm{d}\,\Omega \\ &\quad - \int_{\partial\Omega} \underbrace{\left(\mathbf{grad}\left(\psi\right)\right)\cdot\boldsymbol{n}}_{\boldsymbol{u}\wedge\boldsymbol{n}=u_\tau}\ \boldsymbol{\Phi}\,\mathrm{d}\,\gamma. \end{aligned} \tag{57}$$

Plugging (54)–(55)–(56)–(57) into (53) gives:

$$\begin{cases} \displaystyle\int_\Omega \rho_0\ \mathbf{grad}\left(\partial_t\psi\right)\cdot\mathbf{grad}\left(\varphi\right)\,\mathrm{d}\,\Omega = -\int_\Omega \omega\,\mathbf{grad}^\perp(\psi)\cdot\mathbf{grad}\left(\varphi\right)\,\mathrm{d}\,\Omega \\ \displaystyle + \int_{\partial\Omega}\left(\rho_0\ \partial_t u_\tau + \omega\, u_n\right)\ \varphi\,\mathrm{d}\,\gamma + \int_{\partial\Omega} y_c\ \varphi\,\mathrm{d}\,\gamma, \\ \displaystyle\int_\Omega \mu_c^{-1}\ e_c\ \boldsymbol{\Phi}\,\mathrm{d}\,\Omega = \int_\Omega \mathbf{grad}^\perp(\psi)\cdot\mathbf{grad}^\perp(\boldsymbol{\Phi})\,\mathrm{d}\,\Omega \\ \quad \displaystyle - \int_{\partial\Omega} u_\tau\ \boldsymbol{\Phi}\,\mathrm{d}\,\gamma. \end{cases} \tag{58}$$

Normal and tangential boundary controls for the velocity (u_n and u_τ respectively) are now available in the weak formulation. The observation variable y_c is the colocated boundary observation of the extra control of ψ at the boundary (appearing in (37)), that has to be carefully set for compatibility with the two controls u_n and u_τ. Furthermore, the tangential control appears to require C^1 regularity in time for the resolution. This comes from the substitution of the differential constitutive relation into the dynamical system, as expected.

Let $(\varphi^i)_{i=1,\dots,N_\psi}$, $(\boldsymbol{\Phi}^k)_{k=1,\dots,N_c}$, and $(\xi^m)_{m=1,\dots,N_\partial}$ be three finite element basis of approximation for ψ, e_c, and boundary scalar fields respectively. We denote:

$$\begin{aligned} \psi^d(\boldsymbol{\zeta},t) &:= \sum_{i=1}^{N_\psi} \psi^i(t)\varphi^i(\boldsymbol{\zeta}), & e_c^d(\boldsymbol{\zeta},t) &:= \sum_{k=1}^{N_c} e_c^k(t)\boldsymbol{\Phi}^k(\boldsymbol{\zeta}), \\ u_\square(\boldsymbol{s},t) &:= \sum_{m=1}^{N_\partial} u_\square^m(t)\xi^m(\boldsymbol{s}), & y_c(\boldsymbol{s},t) &:= \sum_{m=1}^{N_\partial} y_c^m(t)\xi^m(\boldsymbol{s}), \end{aligned}$$

the approximations of ψ, e_c, u_n and u_τ, and y_c. Note that we take the same finite element basis at the boundary for the sake of simplicity.

The discrete weak formulation is then given by: taking $\varphi = \varphi^i$ for all $i \in \{1, \dots, N_\psi\}$ and $\Phi = \Phi^k$ for all $k \in \{1, \dots, N_c\}$ as test functions:

$$\begin{bmatrix} M_\psi & 0 \\ 0 & M_c \end{bmatrix} \begin{pmatrix} \underline{\dot{\psi}} \\ \underline{\dot{e}_c} \end{pmatrix} = \begin{bmatrix} J_\omega[\omega^d] & -D \\ D^\top & 0 \end{bmatrix} \begin{pmatrix} \underline{\psi} \\ \underline{e_c} \end{pmatrix} + \begin{bmatrix} B_n[\omega^d] & 0 & B_{\mathrm{d}t} & B_c \\ 0 & B_\tau & 0 & 0 \end{bmatrix} \begin{pmatrix} \underline{u_n} \\ \underline{u_\tau} \\ \underline{\dot{u}_\tau} \\ \underline{y_c} \end{pmatrix}, \tag{59}$$

where $\underline{\square}$ is the collection of the time-dependent coefficients of the approximation $\square^d$ in the associated finite element basis, and:

$$(M_\psi)_{i,j} := \int_\Omega \rho_0 \, \mathbf{grad}(\varphi^j) \cdot \mathbf{grad}(\varphi^i) \, \mathrm{d}\Omega, \qquad (M_c)_{k,\ell} := \int_\Omega \mu_c^{-1} \Phi^\ell \Phi^k \mathrm{d}\Omega,$$

$$(J_\omega[\omega^d])_{i,j} := \int_\Omega \omega^d \ \mathbf{grad}^\perp\left(\varphi^j\right) \cdot \mathbf{grad}\left(\varphi^i\right) \mathrm{d}\Omega,$$

$$(D)_{i,\ell} := \int_\Omega \mathbf{grad}^\perp(\Phi^\ell) \cdot \mathbf{grad}^\perp(\varphi^i) \mathrm{d}\Omega,$$

$$(B_n[\omega^d])_{i,n} := \int_{\partial\Omega} \omega^d \ \xi^n \ \varphi^i \mathrm{d}\gamma, \qquad (B_\tau)_{k,n} := -\int_{\partial\Omega} \xi^n \ \Phi^k \mathrm{d}\gamma,$$

$$(B_{\mathrm{d}t})_{k,n} := \int_{\partial\Omega} \rho_0 \, \xi^n \, \varphi^i \, \mathrm{d}\gamma, \qquad (B_c)_{i,n} := \int_{\partial\Omega} \xi^n \ \varphi^i \mathrm{d}\gamma.$$

Note that $D \in \mathbb{R}^{N_\psi \times N_c}$ is not square in general (as $B_n[\omega^d], B_c, B_{\mathrm{d}t} \in \mathbb{R}^{N_\psi \times N_\partial}$ and $B_\tau \in \mathbb{R}^{N_c \times N_\partial}$).

Remark 13. Interestingly, integration by parts has been here performed on *both* lines, while PFEM usually relies on one integration by parts on the appropriate line (depending on the considered causality).

Dirac-structure and power balance. Let us consider the colocated boundary observations $\underline{y_n}$, $\underline{y_\tau}$ and $\underline{y_{\mathrm{d}t}}$ as well as the colocated control $\underline{u_c}$, obtained by taking the transpose of the big control matrix on the right-hand side of (59):

$$\begin{bmatrix} M_\partial & 0 & 0 & 0 \\ 0 & M_\partial & 0 & 0 \\ 0 & 0 & M_\partial & 0 \\ 0 & 0 & 0 & M_\partial \end{bmatrix} \begin{pmatrix} \underline{y_n} \\ \underline{y_\tau} \\ \underline{y_{\mathrm{d}t}} \\ \underline{u_c} \end{pmatrix} = \begin{bmatrix} B_n[\omega^d]^\top & 0 \\ 0 & B_\tau^\top \\ B_{\mathrm{d}t}^\top & 0 \\ B_c^\top & 0 \end{bmatrix} \begin{pmatrix} \underline{\psi} \\ \underline{e_c} \end{pmatrix},$$

where:

$$(M_\partial)_{m,\ell} := \int_{\partial\Omega} \xi^\ell \ \xi^m \mathrm{d}\gamma,$$

is the boundary mass matrix.

Then, a discrete Dirac structure is given by gathering the above and (59) as follows:

$$\underbrace{\mathrm{Diag}\begin{bmatrix} M_\psi \\ M_c \\ M_\partial \\ M_\partial \\ M_\partial \\ M_\partial \end{bmatrix}}_{\mathbf{M}} \begin{pmatrix} \underline{\dot{\psi}} \\ \underline{\dot{e}_c} \\ -\underline{\dot{y}_n} \\ -\underline{\dot{y}_\tau} \\ -\underline{\dot{y}_{\mathrm{d}t}} \\ \underline{\dot{u}_c} \end{pmatrix} = \underbrace{\begin{bmatrix} J_\omega[\omega^d] & -D & B_n[\omega^d] & 0 & B_{\mathrm{d}t} & -B_c \\ D^\top & 0 & 0 & B_\tau & 0 & 0 \\ -B_n[\omega^d]^\top & 0 & 0 & 0 & 0 & 0 \\ 0 & -B_\tau^\top & 0 & 0 & 0 & 0 \\ -B_{\mathrm{d}t}^\top & 0 & 0 & 0 & 0 & 0 \\ B_c^\top & 0 & 0 & 0 & 0 & 0 \end{bmatrix}}_{\mathbf{J}} \begin{pmatrix} \underline{\psi} \\ \underline{e_c} \\ \underline{u_n} \\ \underline{u_\tau} \\ \underline{\dot{u}_\tau} \\ -\underline{y_c} \end{pmatrix}. \tag{60}$$

This Dirac structure will help computing the power balance satisfied by the discrete Hamiltonian, defined as the continuous one (35) evaluated in the discretization of the energy variable ω^d. Two difficulties arise: first, we recall that ω is implicit in the definition (35), second, we do not have access to $\underline{\omega}$ in our simulation, but to $\underline{\psi}$ and $\underline{e_c}$. Nevertheless, the following proposition holds true.

Proposition 9. *The discrete Hamiltonian can be defined as:*

$$\begin{aligned} \mathcal{H}^d(\underline{\omega}) &= \frac{1}{2} \int_\Omega \rho_0 \left\| \mathbf{grad}\left(\psi^d\right) \right\|^2 \mathrm{d}\Omega, \\ &= \frac{1}{2} \underline{\psi}^\top M_\psi \, \underline{\psi}. \end{aligned} \tag{61}$$

Proof. By definition of the stream function ψ, one has $\boldsymbol{u} = \mathbf{grad}^\perp(\psi)$. At the discrete level, this reads $\boldsymbol{u}^d = \mathbf{grad}^\perp(\psi^d)$, hence:

$$\mathcal{H}^d(\underline{\omega}) = \frac{1}{2} \int_\Omega \rho_0 \left\| \mathbf{grad}^\perp\left(\psi^d\right) \right\|^2 \mathrm{d}\Omega,$$

holds. Furthermore, a trivial computation shows that $\left\| \mathbf{grad}^\perp\left(\psi^d\right) \right\|^2 = \left\| \mathbf{grad}\left(\psi^d\right) \right\|^2$, leading to the first claimed equality. Replacing $\psi^d(\boldsymbol{\zeta}, t)$ by the sum $\sum_{i=1}^{N_\psi} \psi^i(t) \varphi^i(\boldsymbol{\zeta})$ gives the second claimed equality. □

Remark 14. The discretization $\boldsymbol{u}^d$ of the velocity field as defined above is consistent with both the discrete stream function ψ^d (by definition) and the discrete vorticity ω^d. Indeed, ω^d must satisfy $\omega^d = \mathrm{curl}_{2D} \boldsymbol{u}^d$, which becomes $\omega^d = \mathrm{curl}_{2D} \mathbf{grad}^\perp(\psi^d) = -\Delta\psi^d$ (in a weak sense), *i.e.* the constitutive relation that has been used to eliminate ω^d.

Remark 15. The "mass" matrix M_ψ is a stiffness-like matrix in this particular case where the constitutive relation $-\Delta\psi = \omega$ has been embedded into the dynamical system. It is not positive-definite, however, the big block diagonal "mass" matrix $\mathbf{M}$ on the left-hand side of the Dirac structure (60) is positive-definite as soon as the initial value of the boundary control $\underline{u_c}(0)$ is compatible with the initial value of $\underline{\phi}(0)$, *i.e.,* on:

$$X := \left\{ \begin{pmatrix} \underline{\psi}^\top & \underline{e_c}^\top & -\underline{y_n}^\top & -\underline{y_\tau}^\top & -\underline{y_{\mathrm{d}t}}^\top & \underline{u_c}^\top \end{pmatrix}^\top \in \mathbb{R}^{N_\psi + N_c + 4N_\partial} \mid B_c^\top \underline{\psi} = M_\partial \underline{u_c} \right\},$$

as a subspace of $\mathbb{R}^{N_\psi + N_c + 4N_\partial}$. Indeed, one has a symmetric positive matrix. Assume that $\begin{pmatrix} \underline{\psi}^\top & \underline{e_c}^\top & -\underline{y_n}^\top & -\underline{y_\tau}^\top & -\underline{y_{\mathrm{d}t}}^\top & \underline{u_c}^\top \end{pmatrix}^\top \in \mathrm{Ker}\mathbf{M} \subset X$, then $M_\psi \underline{\psi} = 0$. Now, recall that:

$$(M_\psi)_{i,j} := \int_\Omega \rho_0 \, \mathbf{grad}(\varphi^j) \cdot \mathbf{grad}(\varphi^i) \, \mathrm{d}\Omega,$$

hence, $M_\psi \underline{\psi} = 0$ implies that ψ^d is constant (and the associated velocity field $\boldsymbol{u}^d$ is null). Since on the kernel, $M_\partial \underline{u_c} = 0$, one has $B_c^\top \psi = 0$ in X. Or in other words: the Dirichlet trace of ψ^d is identically zero, implying that the constant approximated function ψ^d is identically zero. Finally, this proves that $\mathrm{Ker}\mathbf{M} = \{0\}$ on X, hence $\mathbf{M}$ is positive-definite.

With Proposition 9 and the discrete Dirac structure (60) at hand, the power balance can be computed.

Theorem 10. *Let $(\underline{\psi}, \underline{e_c}, \underline{y_n}, \underline{y_\tau}, \underline{y_{\mathrm{d}t}}, \underline{y_c})$ be a trajectory, i.e., a solution to (60) for some initial data and compatible controls $\underline{u_n} \in C^0(0, \infty; \mathbb{R}^{N_\partial})$, $\underline{u_\tau} \in C^1(0, \infty; \mathbb{R}^{N_\partial})$ and $\underline{u_c} \in C^0(0, \infty; \mathbb{R}^{N_\partial})$. Then the following power balance holds true for $t \geq 0$:*

$$\frac{\mathrm{d}}{\mathrm{d}t} \mathcal{H}^d(\underline{\omega}) = -\underline{e_c}^\top M_c \, \underline{e_c} + \underline{u_n}^\top M_\partial \, \underline{y_n} + \underline{u_\tau}^\top M_\partial \, \underline{y_\tau} + \underline{y_c}^\top M_\partial \, \underline{u_c}, \tag{62}$$

which preserves the power balance (37) at the discrete level.

Proof. See Appendix B.4 □

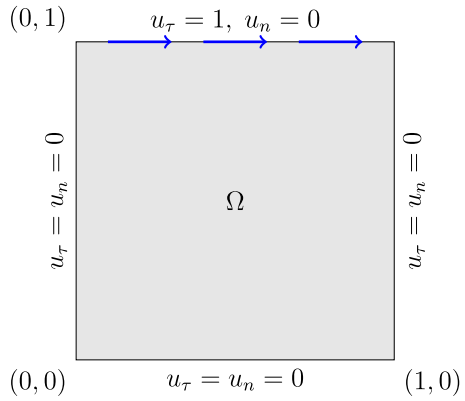

Fig. 4. The configuration of the lid-driven cavity test case.

Numerical results for the lid-driven cavity problem

The vorticity-stream function formulation allows for the simulation to be done at a reduced cost. To test its precision, let us consider the lid-driven cavity problem, for which benchmarks can be found at the following address: http://www.zetacomp.com, and are addressed in [58].

The lid-driven cavity problem is a particular 2D test case where the fluid fills a unit square and is controlled tangentially by the upper boundary of the square at a constant velocity of 1 m s^{-1}, see Fig. 4.

In the sequel, the simulations are performed in python, using GMSH [57] as mesh generator, FEniCS [85] as finite element library and PETSc [1] for the time integration of the resulting nonlinear DAE. The meshes are refined near the upper corners of the square, as the highest velocity variations (hence, values for the vorticity), will occur at these spots. In all the simulations, the initial data are identically null, and the boundary control is constant and applied as soon as $t > 0$. Videos of these simulations can be downloaded in https://nextcloud.isae.fr/index.php/s/4TrMBSZa86cL6w2.

Reynolds 100. The first simulations are done at Reynolds 100, *i.e.*, for a fluid of mass density $\rho_0 \equiv 1$, with a viscosity $\mu = 1.e^{-2}$. At this Reynolds number, one vortex takes place in the square.

The finite element families are chosen as follows: continuous Lagrange finite elements of order 2 $\mathbb{P}^2$ for the co-energy variable ψ, continuous Lagrange finite elements of order 1 $\mathbb{P}^1$ for the effort variable e_c, and boundary continuous Lagrange finite elements of order 1 $\mathbb{P}^1$ for all boundary fields.

The discretization of the square leads to about 10,000 degrees of freedom. One may appreciate how the streamlines are recovered when the dynamical system reaches the stationary solution, as can be observed in Fig. 5.

Reynolds 400. The viscosity is lowered at $\mu = 2.5e^{-3}$. At this Reynolds number, a first recirculation area appears in the lower-right corner of the square.

The finite element families are chosen as for the case $\mu = 1.e^{-2}$.

The simulation requires a finer discretization of the domain to capture the higher variations of velocity in the fluid, which leads to 40,000 degrees of freedom. Fig. 6 shows the development of the two vortices, and how the chosen strategy allows recovering the evolution to the stationary solution.

Reynolds 1000. Now, the viscosity is $\mu = 1.e^{-3}$. At this Reynolds number, a second recirculation area appears in the lower-left corner of the square.

The finite elements families are chosen as follows: continuous Lagrange finite elements of order 3 $\mathbb{P}^3$ for the co-energy variable ψ, continuous Lagrange finite elements of order 2 $\mathbb{P}^2$ for the effort variable e_c, and boundary continuous Lagrange finite elements of order 1 $\mathbb{P}^1$ for all boundary fields.

The discretization is again finer than previously, once more, to consider higher variations in the velocity field. To improve the numerical behavior near the first recirculation area, the lower-right corner is also refined. These refinements and higher orders of finite elements lead to a nonlinear DAE of size 360,000. One may see in Fig. 7 the efficiency of the proposed approach: both recirculation areas are captured, and the center of the main vortex is well-recovered.

Remark 16. Discretizing the velocity–vorticity–pressure formulation (31) would have required about one million degrees of freedom to reach the same precision (even after substitution of the constitutive relation $\boldsymbol{e}_c = \mu_c \boldsymbol{f}_c$ into (31), as $\boldsymbol{f}_c = \mu_c^{-1}\boldsymbol{e}_c$). In this 2D setting, the computational burden has been significantly reduced by using the vorticity–stream function formulation (52), while preserving the underlying geometric structure of the physical phenomena at the discrete level.

4. Extension to thermodynamics

If thermal phenomena cannot be neglected then the thermal domain needs to be taken into account in the model. This Section focuses on Irreversible pH (IpH) systems, which is a specific thermodynamic formulation closely related to dissipative pH systems. It is shown how by relating the dissipative ports of a pH system with the *entropy production* a quasi pH structure arises which assures both energy conservation and irreversible entropy creation. Furthermore, by introducing a class of pseudo-bracket it is possible to precisely parametrize the quasi pH structure by the thermodynamic driving forces which induce the irreversible phenomena in the system. The developments are illustrated by systematically developing the 1D SWE.

4.1. Quasi pH system

Recall the formulation of dissipative pH systems which are of the form $\partial_t \boldsymbol{x}(\boldsymbol{\zeta}, t) = \mathcal{J}\delta_{\boldsymbol{x}}\mathcal{H} - \mathcal{G}S\mathcal{G}^*\delta_{\boldsymbol{x}}\mathcal{H}$, where $\mathcal{G}$ is a differential operator and $\mathcal{G}^*$ the corresponding formal adjoint, and $S \geq 0$ is a non-negative bounded matrix operator of appropriate dimensions. In this case, $\mathcal{G}S\mathcal{G}^*$ represents the dissipation and can be split into two parts such to express the dissipative pH system from an extended Dirac structure as

$$\begin{pmatrix} \partial_t \boldsymbol{x}(\boldsymbol{\zeta}, t) \\ \boldsymbol{f}_d \end{pmatrix} = \underbrace{\begin{bmatrix} \mathcal{J} & \mathcal{G} \\ -\mathcal{G}^* & 0 \end{bmatrix}}_{\widetilde{\mathcal{J}}} \begin{pmatrix} \boldsymbol{e} \\ \boldsymbol{e}_d \end{pmatrix}, \text{ with } \boldsymbol{e}_d = S\boldsymbol{f}_d, \tag{63}$$

$$\begin{pmatrix} \boldsymbol{f}_\partial \\ \boldsymbol{e}_\partial \end{pmatrix} = \widetilde{\mathcal{W}}_{\partial\Omega} \begin{pmatrix} \boldsymbol{e}|_{\mathrm{d}\,\Omega} \\ \boldsymbol{e}_d|_{\mathrm{d}\,\Omega} \end{pmatrix}, \tag{64}$$

where $\partial_t \boldsymbol{x}(\boldsymbol{\zeta}, t) \in \mathcal{F}$ and $S > 0$. $\widetilde{\mathcal{J}}$ is an extended formally skew-symmetric differential operator, $\boldsymbol{f}_\partial$ and $\boldsymbol{e}_\partial$ are the boundary flow and effort port variables, $\widetilde{\mathcal{W}}_{\partial\Omega}$ is an operator dependent on the unitary vector $\boldsymbol{n}$ outward to $\partial\Omega$, that describes the normal and tangential projections on $\partial\Omega$, induced by $\widetilde{\mathcal{J}}$, of the co-energy variables $\boldsymbol{e} := \delta_{\boldsymbol{x}}\mathcal{H}$ and dissipative effort $\boldsymbol{e}_d$, such that,

$$\dot{\mathcal{H}} = \int_{\partial\Omega} \boldsymbol{f}_\partial \cdot \boldsymbol{e}_\partial \,\mathrm{d}\gamma - \int_\Omega \boldsymbol{f}_d \cdot \boldsymbol{e}_d \,\mathrm{d}\,\Omega, \tag{65}$$

where $\int_{\partial\Omega} \boldsymbol{f}_\partial \cdot \boldsymbol{e}_\partial \,\mathrm{d}\gamma$ describes the power supplied to the system through the boundaries and $\int_\Omega \boldsymbol{f}_d \cdot \boldsymbol{e}_d \,\mathrm{d}\,\Omega$ the power dissipated into heat by the internal phenomena (such as friction or viscosity). As discussed in Section 2.2, the formulation (63) is very convenient for numerical approximations [91], since the extended operator $\widetilde{\mathcal{J}}$ is linear. However, the resolution of the system dynamics is implicit since the dissipative port introduce an algebraic constraint.

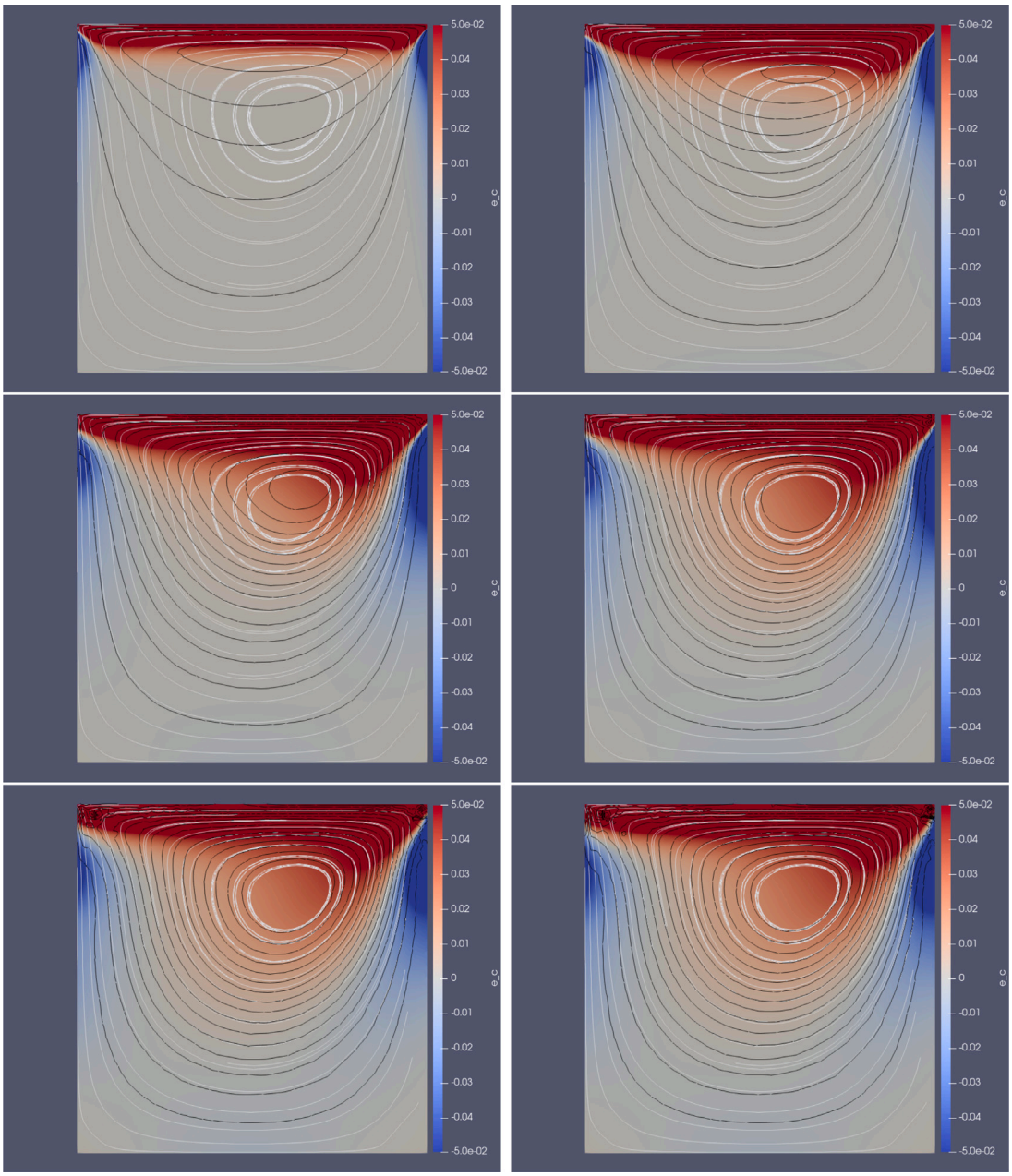

Fig. 5. Lid-driven cavity problem at Reynolds 100 ($\mu = 1.e^{-2}$) at times $t = 0.1, 0.5, 2, 4, 8$, and 10 s. The color represents the effort variable $e_c = \mu\omega$, while the solid black lines are streamlines, to compare with the white streamlines from [58].

In the case of the dissipative SWE example, the formulation (63) is of the form

$$\begin{pmatrix} \partial_t q \\ \partial_t \alpha \\ f_d \end{pmatrix} = \begin{pmatrix} 0 & -\partial_\zeta & 0 \\ -\partial_\zeta & 0 & 1 \\ 0 & -1 & 0 \end{pmatrix} \begin{pmatrix} e_q \\ e_\alpha \\ e_d \end{pmatrix}, \tag{66}$$

with $e_d = S f_d$ and with power balance given by

$$\dot{\mathcal{H}} = -\int_{[0,L]} S {f_d}^2 \mathrm{d}\zeta + \boldsymbol{e}_\partial^T \boldsymbol{f}_\partial = -\int_{[0,L]} S {e_\alpha}^2 \mathrm{d}\zeta + \boldsymbol{e}_\partial^T \boldsymbol{f}_\partial, \tag{67}$$

where $\mathcal{G} = [0\ 1]^\top$ and $S = S(q, \alpha) \geq 0$ is a nonlinear function of the energy variables q and α.

Regarding the general formulation (63), if $\mathcal{G} = 0$, then the boundary controlled system is energy preserving or reversible. If $\mathcal{G} \neq 0$ the system is dissipative, meaning that energy is being transformed into heat by some dissipative phenomena, such as mechanical friction. Note that these implicit formulations have been recently extended to pH systems formulations defined on Lagrange submanifolds, to cope with a larger class of systems involving an implicit definition of the energy [136,137].

An alternative approach consists in representing explicitly the thermal domain in the system formulation using the entropy density variable s and the total energy [132], preferably to the mechanical, electrical or magnetic energies. In this case, the total energy of the system can be split as the sum of the mechanical, electrical or magnetic energy (or the sum of them) and the internal energy $\int_{[0,L]} e(s)\mathrm{d}\zeta$:

$$H(\boldsymbol{x}, s) = \mathcal{H}(\boldsymbol{x}) + \int_{[0,L]} e(s)\mathrm{d}\zeta,$$

where s is the entropy per unit length. From the first law, in the absence of exchange of energy with the surroundings, i.e. $\boldsymbol{e}_\partial \boldsymbol{f}_\partial = 0$, the total energy is preserved, implying:

$$\dot{H} = \dot{\mathcal{H}} + \int_{[0,L]} \dot{e}(s)\mathrm{d}\zeta = 0,$$

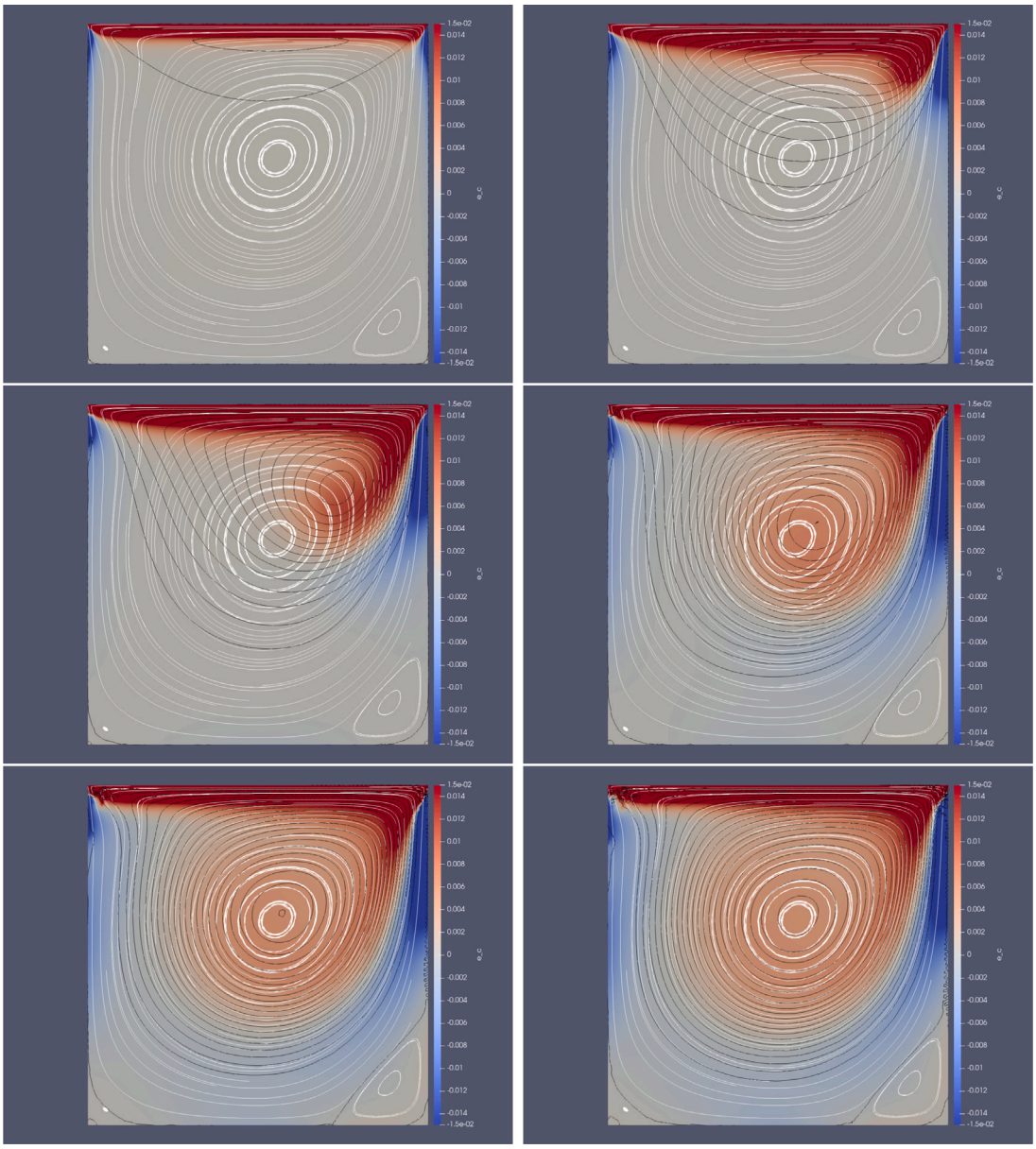

Fig. 6. Lid-driven cavity problem at Reynolds 400 ($\mu = 2.5e^{-3}$) at times $t = 0.1, 1, 3, 7, 12$, and 18 s. The color represents the effort variable $e_c = \mu\omega$, while the solid black lines are streamlines, to compare with the white streamlines from [58].

$$= \int_{[0,L]} (-f_d\, e_d + \partial_s e\, \partial_t s)\, \mathrm{d}\zeta = 0,$$
$$= \int_{[0,L]} \left(-\delta_{\boldsymbol{x}} \mathcal{H}\, (\mathcal{G}S\mathcal{G}^*)\, \delta_{\boldsymbol{x}} \mathcal{H} + \partial_s e\, \partial_t s\right)\, \mathrm{d}\zeta = 0.$$

Noticing that $\delta_{\boldsymbol{x}} \mathcal{H} = \delta_{\boldsymbol{x}} H$ and recalling from Gibbs' fundamental relation that the temperature is a function of the entropy, in this case $T = \partial_s e$, the internal entropy creation density, σ, of the system is explicitly written as:

$$\partial_t s = \frac{1}{T} \delta_{\boldsymbol{x}} H^T\, (\mathcal{G}S\mathcal{G}^*)\, \delta_{\boldsymbol{x}} H = \sigma \geq 0,$$

in accordance with the second law of Thermodynamics. The resulting system is then:

$$\begin{bmatrix} \partial_t \boldsymbol{x} \\ \partial_t s \end{bmatrix} = \begin{bmatrix} \mathcal{J} & -(\mathcal{G}S\mathcal{G}^*)\, \delta_{\boldsymbol{x}} \mathcal{H} \frac{1}{T} \\ \frac{1}{T} \delta_{\boldsymbol{x}} H^\top\, (\mathcal{G}S\mathcal{G}^*)^* & 0 \end{bmatrix} \begin{bmatrix} \delta_{\boldsymbol{x}} H \\ T \end{bmatrix}, \tag{68}$$

which corresponds to a quasi pH system [116], since it resembles a pH system, but its structure matrix operator is a function of the gradient of the energy. The formulation (68) allows to explicitly solve the dynamic equations of the system. However, the symplectic structure of the pH system, given by the Poisson tensor associated with the structure matrix, is now destroyed, and the structure matrix is no longer linear; hence the numerical schemes discussed in previous sections need to be rethought. In order to illustrate this new formulation with a concrete example, consider again the dissipative 1D SWE of Section 2.3.1. Its quasi pH system formulation is:

$$\begin{pmatrix} \partial_t q \\ \partial_t \alpha \\ \partial_t s \end{pmatrix} = \begin{pmatrix} 0 & -\partial_\zeta & 0 \\ -\partial_\zeta & 0 & -\frac{S}{T} e_\alpha \\ 0 & \frac{S}{T} e_\alpha & 0 \end{pmatrix} \begin{pmatrix} e_q \\ e_\alpha \\ T \end{pmatrix}. \tag{69}$$

The formulation (69) allows to explicitly characterize the irreversible dynamic of SWE. Indeed, the last coordinate gives the precise expression of the internal entropy creation. For instance, when considering the Darcy–Weisbach water-bed friction model $S = \frac{f_{DW}\, b|\alpha|}{8q}$, with f_{DW} the empirical friction coefficient, the internal entropy creation is:

$$\partial_t s = \frac{S}{T} {e_\alpha}^2 = \frac{1}{T} \frac{f_{DW}\, b|\alpha|}{8q} \left(\frac{q\alpha}{\rho}\right)^2 \geq 0.$$

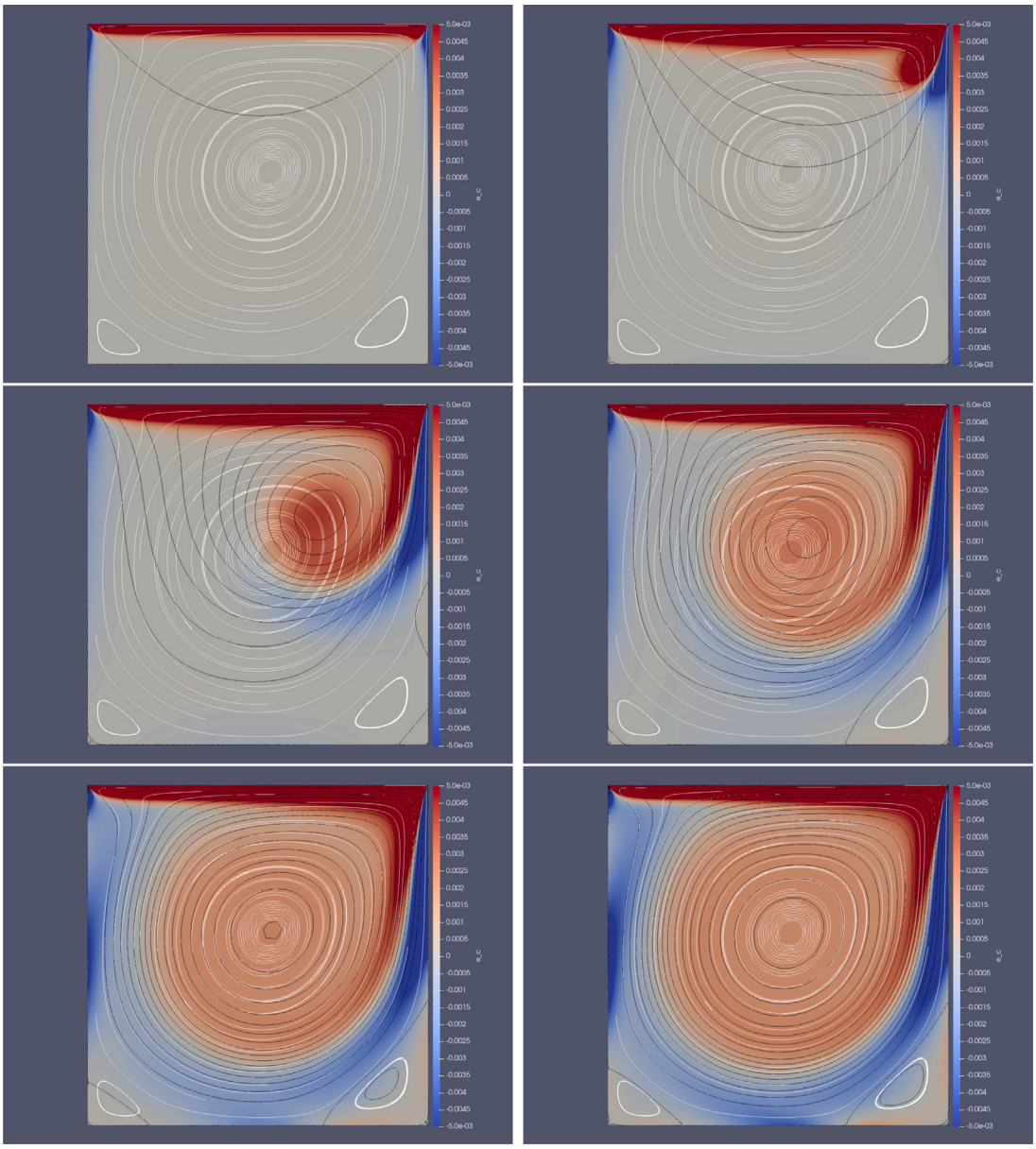

Fig. 7. Lid-driven cavity problem at Reynolds 1000 ($\mu = 1.e^{-3}$) at times $t = 0.1, 1, 5, 10, 18$, and 35 s. The color represents the effort variable $e_c = \mu\omega$, while the solid black lines are streamlines, to compare with the white streamlines from [58].

4.2. Irreversible port-Hamiltonian systems

IpH systems were defined [116] as an extension of pH systems for the purpose of representing not only the energy balance but also the entropy balance, essential in thermodynamics, as a structural property of a system. The extension of this framework to infinite-dimensional systems defined on 1D spatial domains with first order differential operators was proposed in [113] for a class of diffusion processes and generalized for a large class of thermodynamic systems in [115]. The main feature of the IpH systems formulation is that it precisely parametrizes the operators of (68) in terms of the thermodynamic properties of a system such that, similar to pH systems, the structure matrices of the system have a clear physical interpretation.

We shall define the following pseudo-brackets[9] for any two functionals H_1 and H_2 of and for any matrix differential operator $\mathcal{G}$ as:

$$\begin{aligned}\left\{H_1|\mathcal{G}|H_2\right\} &= \begin{bmatrix}\delta_{\boldsymbol{x}} H_1 \\ \delta_s H_1\end{bmatrix} \cdot \begin{bmatrix}0 & \mathcal{G} \\ -\mathcal{G}^* & 0\end{bmatrix} \begin{bmatrix}\delta_{\boldsymbol{x}} H_2 \\ \delta_s H_2\end{bmatrix}, \\ \left\{H_1|H_2\right\} &= \delta_s H_1^\top \left(\partial_\zeta \delta_s H_2\right),\end{aligned} \tag{70}$$

where $\mathcal{G}^*$ denotes the formal adjoint operator of $\mathcal{G}$. An IpH system undergoing m irreversible processes on a 1D spatial domain is defined by a total energy and total entropy functional, respectively H and S, a pair of matrices $P_0 = -P_0^\top \in \mathbb{R}^{n\times n}$, $P_1 = P_1^\top \in \mathbb{R}^{n\times n}$, $G_0 \in \mathbb{R}^{n\times m}$, $G_1 \in \mathbb{R}^{n\times m}$ with $m \leq n$ and the strictly positive real-valued functions $\gamma_{k,i}\left(\boldsymbol{x}, \zeta, \delta_{\boldsymbol{x}} H\right)$ $k = 0, 1$; $i \in \{1, \dots m\}$, $\gamma_s\left(\boldsymbol{x}, \zeta, \delta_{\boldsymbol{x}} H\right) > 0$ and the PDE:

$$\begin{bmatrix}\partial_t \boldsymbol{x} \\ \partial_t s\end{bmatrix} = \begin{bmatrix}\mathcal{J} & \mathcal{G}_{\mathcal{R}} \\ \mathcal{G}_{\mathcal{R}}^* & \mathbf{r_s}\partial_\zeta + \partial_\zeta\left(\mathbf{r_s}\cdot\right)\end{bmatrix} \begin{bmatrix}\delta_{\boldsymbol{x}} H \\ \delta_s H\end{bmatrix},$$

where:

$$\mathcal{J} = P_0 + P_1\partial_\zeta, \quad \mathcal{G}_{\mathcal{R}} = G_0\mathbf{R_0} + \partial_\zeta\left(G_1\mathbf{R}_1\cdot\right), \quad \mathcal{G}_{\mathcal{R}}^* = -\mathbf{R}^\top G_0^\top + \mathbf{R}_1^\top G_1^\top \partial_\zeta,$$

with vector-valued functions $\mathbf{R}_l\left(\boldsymbol{x}, \delta_{\boldsymbol{x}} H\right) \in \mathbb{R}^{m\times 1}$, $l = 0, 1$, defined by:

$$R_{0,i} = \gamma_{0,i}\left(\boldsymbol{x}, \zeta, \delta_{\boldsymbol{x}} H\right)\left\{S|G_0(:,i)|H\right\},$$

[9] the bracket is called a pseudo-bracket in the sense that the Jacobi-identity is not automatically satisfied, see e.g. [134,135] for more details.

$$R_{1,i} = \gamma_{1,i}\left(\boldsymbol{x}, \zeta, \delta_{\boldsymbol{x}} H\right)\left\{S|G_1(:,i)\partial_\zeta|H\right\},$$

and:

$$r_s = \gamma_s\left(\boldsymbol{x}, \zeta, \delta_{\boldsymbol{x}} H\right)\{S|H\},$$

where the notation $G(:,i)$ indicates the ith column of the matrix G. Here the operator $\mathcal{J}$ corresponds to the reversible coupling phenomena as it appears in the example of the 1D SWE $P_0 = 0$ and: $P_1 = \begin{bmatrix} 0 & -1 \\ -1 & 0 \end{bmatrix}$. The operator $\mathcal{G}_{\mathcal{R}}$ corresponds to the irreversible coupling phenomena. In the example of the dissipative 1D SWE, $G_0 = 0$ and: $G_1 = \begin{bmatrix} 0 \\ 1 \end{bmatrix}$ which indicates that the irreversible phenomenon associated with the friction of the fluid, couples the momentum and the entropy balance equations. The functions $\gamma_{k,i}$ and γ_s define the constitutive relations of the irreversible phenomena and the functions $\left\{S|G_0(:,i)|H\right\}$, $\left\{S|G_1(:,i)\partial_\zeta|H\right\}$ and $\{S|H\}$ correspond to their driving forces. In the example of the dissipative 1D SWE, $\left\{S|G_1(:,i)\partial_\zeta|H\right\} = e_\alpha = \frac{q\alpha}{\rho}$ is indeed the driving force of the friction and $\gamma_{1,1} = \frac{S}{T}$ with $T = \delta_s H$ is indeed a strictly positive function containing the friction coefficient and defining the constitutive relation of the friction model.

The previous definition is completed with port variables which enable to write the interaction of the system with its environment or other physical systems, in the manner as for dissipative pH systems as presented in Section 2.2. To this end, a Boundary Controlled IpH systems (BC-IPHS) is an infinite-dimensional IpH systems augmented with the boundary port variables:

$$v(t) = W_B \begin{bmatrix} e(L,t) \\ e(0,t) \end{bmatrix}, \qquad y(t) = W_C \begin{bmatrix} e(L,t) \\ e(0,t) \end{bmatrix}, \tag{71}$$

as linear functions of the modified effort variable:

$$e(t,z) = \begin{bmatrix} \delta_{\boldsymbol{x}} H \\ \mathbf{R}\,\delta_s H \end{bmatrix}, \tag{72}$$

with $\mathbf{R} = \begin{bmatrix} 1 & \mathbf{R_1} & \mathbf{r_s} \end{bmatrix}^\top$ and:

$$W_B = \begin{bmatrix} \frac{1}{\sqrt{2}}\left(\Xi_2 + \Xi_1 P_{ep}\right) M_p & \frac{1}{\sqrt{2}}\left(\Xi_2 - \Xi_1 P_{ep}\right) M_p \end{bmatrix},$$
$$W_C = \begin{bmatrix} \frac{1}{\sqrt{2}}\left(\Xi_1 + \Xi_2 P_{ep}\right) M_p & \frac{1}{\sqrt{2}}\left(\Xi_1 - \Xi_2 P_{ep}\right) M_p \end{bmatrix},$$

where $M_p = \left(M^\top M\right)^{-1} M^\top$, $P_{ep} = M^\top P_e M$ and $M \in \mathbb{R}^{(n+m+2)\times k}$ is spanning the columns of $P_e \in \mathbb{R}^{n+m+2}$ of rank k, defined by:

$$P_e = \begin{bmatrix} P_1 & 0 & G_1 & 0 \\ 0 & 0 & 0 & g_s \\ G_1^\top & 0 & 0 & 0 \\ 0 & g_s & 0 & 0 \end{bmatrix}, \tag{73}$$

and where Ξ_1 and Ξ_2 in $\mathbb{R}^{k\times k}$ satisfy $\Xi_2^\top \Xi_1 + \Xi_1^\top \Xi_2 = 0$ and $\Xi_2^\top \Xi_2 + \Xi_1^\top \Xi_1 = I$. Recalling the dissipative 1D SWE, its BC-IPHS formulation is obtained by completing the model with the boundary port variables:

$$v(t) = \begin{bmatrix} -e_q(L,t) + \frac{S}{T} e_\alpha(L,t) \\ e_q(0,t) - \frac{S}{T} e_\alpha(0,t) \end{bmatrix} = \begin{bmatrix} -\left(\frac{\alpha^2}{2\rho} + \frac{\rho g}{b} q\right)(L,t) + \frac{S}{T}\frac{q\alpha}{\rho}(L,t) \\ \left(\frac{\alpha^2}{2\rho} + \frac{\rho g}{b} q\right)(0,t) - \frac{S}{T}\frac{q\alpha}{\rho}(0,t) \end{bmatrix},$$
$$y(t) = \begin{bmatrix} e_\alpha(L,t) \\ e_\alpha(0,t) \end{bmatrix} = \begin{bmatrix} \frac{q\alpha}{\rho}(L,t) \\ \frac{q\alpha}{\rho}(0,t) \end{bmatrix}.$$

As for the reversible case, the boundary inputs and outputs correspond, respectively, to the pressure and the velocity evaluated at the boundary points 0 and L. Note however that this time the pressure is the sum of the static and hydrodynamic pressures. If there is no dissipation in the system, $S = 0$, then the boundary inputs and outputs are exactly the same as for the reversible case.

BC-IPHS encode the first and second laws of Thermodynamics, *i.e.*, the conservation of the total energy and the irreversible production of entropy, as stated in the following lemmas [114,115].

Lemma (*First Law Of Thermodynamics*)**.** The total energy balance is:

$$\dot{H} = y(t)^\top v(t),$$

which leads, when the input is set to zero, to $\dot{H} = 0$ in accordance with the first law of Thermodynamics.

Lemma (*Second Law Of Thermodynamics*)**.** The total entropy balance is given by:

$$\dot{S} = \int_{[0,L]} \sigma_t \mathrm{d}\zeta - y_S^\top v_s,$$

where y_s and v_s are entropy conjugated input/output and σ_t is the total internal entropy production. This leads, when the input is set to zero, to $\dot{S} = \int_{[0,L]} \sigma_t \mathrm{d}\zeta \geq 0$ in accordance with the second law of Thermodynamics.

4.3. Multidimensional fluids and relation with metriplectic systems

The infinite-dimensional IpH systems formulation has to date been developed for systems defined on 1D spatial domains. In [96] the pH systems framework was applied to model 3D compressible fluids, both isentropic and non-isentropic. For isentropic fluids, a dissipative pH system model that accounts for the conversion of kinetic energy into heat due to viscous friction was proposed, incorporating dissipative terms linked to the flow's vorticity and compressibility. In scenarios involving fluid mixtures with multiple chemical reactions under non-isentropic conditions, a quasi pH systems formulation was employed to capture the dynamics and thermodynamic behavior of the fluid. This approach involves defining specific operators and their formal adjoints to characterize the various physical phenomena, including boundary conditions related to the diffusion flux of matter. These results extended previous pH systems formulations for non-isentropic 1D fluids [4,98] to 2D and 3D spatial domains, marking initial steps towards a general IpH systems formulation for complex fluids and much in line with other geometrically consistent thermodynamic formulations [25–27].

Recently, in [95] these developments were further generalized and formalized to establish a comprehensive 1, 2, and 3D IpH systems formulation for compressible fluids. This involves precise definition of operators that determine the IpH systems structure and boundary variables, ensuring compliance with the first and the second law of Thermodynamics. The thermodynamic formulation of fluids necessarily leads to the definition of metriplectic dynamics [100] or similarly the GENERIC framework [62,108]. This formulation is a comprehensive approach in thermodynamics that aims at describing both equilibrium and non-equilibrium systems. At its core it was proposed for closed systems and consists of a reversible part that is governed by a Poisson bracket, and an irreversible part governed by a dissipation bracket. These two parts are connected via energy and co-energy variables that describe the system. The reversible part captures the conservative dynamics typically associated with Hamiltonian mechanics, while the irreversible part accounts for dissipative phenomena, such as heat flow and viscous damping. By combining these two aspects, GENERIC provides a unified description of the dynamics of complex systems, encompassing both reversible and irreversible processes, and can be applied to a wide range of physical situations, from fluid dynamics to chemical reactions. There have been several studies in the last decades extending GENERIC to open systems by establishing the link of the formalism with other geometric approaches, such as the Matrix Model [45,74] and networked controlled systems defined by Dirac structures [75]. More recently, the link with dissipative pH systems have been established in [86,102] when considering the *Exergy* of a thermodynamic system as the Hamiltonian function. Regarding numerical discretization schemes, recent works have tackled the structure-preserving discretization in space and time of metriplectic systems [78,107,122].

These results, which relate the different Hamiltonian-based formulations are promising since they establish bridges between the approaches

in terms of fundamental thermodynamic principles, which are expected to help in the developments and the extension of powerful proven numerical schemes such as PFEM for quasi pH systems and IpH systems formulations of thermodynamic systems.

Conclusion and perspectives

In conclusion, this paper has provided an extensive survey and analysis of port-Hamiltonian formulations for the modeling and numerical simulation of open-fluid systems.

The focal point of our discussion has been on the application of port-Hamiltonian formulations to the shallow water equations and the incompressible Navier–Stokes equations in 2D. Starting from the continuous formulation with non-quadratic Hamiltonian, the application of a structure-preserving method needed to be adapted with care, and was not straightforward contrarily to the linear quadratic features of structural mechanics: either a polynomial nonlinearity or a differential linearity in the constitutive relation have been successfully tackled. Through the presentation of numerical simulation results for these specific cases, we have demonstrated the effectiveness of the framework in capturing the essential dynamics of fluid systems.

Beyond these specific applications, our work has highlighted the broader implications of port-Hamiltonian formulations. Notably, it points towards promising research directions in the realm of thermodynamically-consistent modeling, structure-preserving numerical methods and also boundary control design for fluids. This, in turn, sets the stage for the simulation of complex fluid systems in interaction with their environment.

Addressing advanced constitutive laws, particularly for non-Newtonian fluids, stands as a significant challenge and an avenue for future investigation. Additionally, the intricate dynamics of fluid–structure interaction presents complexities, such as the interplay between Lagrangian and Eulerian coordinates and the temporal evolution of the boundary between the fluid and the structure. Tackling these issues opens new frontiers for research, promising advances in our understanding and simulation capabilities for fluid systems.

CRediT authorship contribution statement

Flávio Luiz Cardoso-Ribeiro: Writing – review & editing, Writing – original draft. **Ghislain Haine:** Writing – review & editing, Writing – original draft. **Yann Le Gorrec:** Writing – review & editing, Writing – original draft. **Denis Matignon:** Writing – review & editing, Writing – original draft. **Hector Ramirez:** Writing – review & editing, Writing – original draft.

Declaration of competing interest

The authors declare that they have no known competing financial interests or personal relationships that could have appeared to influence the work reported in this paper.

Data availability

All the codes that are used to perform the simulations will be freely available.

Acknowledgments

The authors would like to warmly thank all the direct contributors to these works; first of all the Ph.D. students and post-doctoral researchers who have been working with lot of professionalism and enthusiasm on these topics, namely Andrea Brugnoli, Luis A. Mora, Anass Serhani, Saïd Aoues, Florian Monteghetti, Antoine Bendimerad-Hohl. They also want to thank their regular collaborators for their contributions, insight and support, namely Paul Kotyczka, Laurent Lefèvre, Valérie Budinger, Daniel Alazard, Thomas Hélie, Michel Fournié. They are also very grateful to their colleagues that deeply contributed and put lot of energy to settle and move forward this field of research for their fruitful discussions and inspiration Bernhard Maschke, Arjan van der Schaft, Stefano Stramigioli, Hans Zwart, Volker Mehrmann among others.

The authors also gratefully acknowledge the funding support of the Agence de l'Innovation de Défense (AID), grant FAMAS (2020 65 0058); the Agence Nationale de la Recherche (ANR), grants EIPHI Graduate School (ANR-17-EURE-0002) and IMPACTS (ANR-21-CE48-0018); the Agencia Nacional de Investigación y Desarrollo (ANID), grants ECOS-ANID (C22E01/220040), FONDECYT (1231896), and Basal (FB0008); and the Coordenação de Aperfeiçoamento de Pessoal de Nível Superior - Brasil (CAPES), grant Brafitec (88887.717002/2022-00).

Appendix A. Some useful definitions

Definition 3 (*Formal Adjoint*)**.** Given a differential operator $\mathcal{A} : D(\mathcal{A}) \subset \mathcal{X} \to \mathcal{Y}$, where $\mathcal{X}$ and $\mathcal{Y}$ are two Hilbert spaces (of functions), the formal adjoint $\mathcal{A}^*$ of $\mathcal{A}$ is defined as:

$$\int_\Omega \mathcal{A}\varphi \cdot \psi \, \mathrm{d}\Omega =: \int_\Omega \varphi \cdot \mathcal{A}^*\psi \, \mathrm{d}\Omega, \qquad \forall \varphi, \psi \in C_c^\infty(\Omega),$$

where $C_c^\infty(\Omega)$ is the space of compactly-supported infinitely differentiable functions.

Definition 4 (*Formal Skew-Symmetry*)**.** A differential operator $\mathcal{J} : D(\mathcal{J}) \subset \mathcal{X} \to \mathcal{X}$ is formally skew-symmetric if:

$$\int_\Omega \mathcal{J}\varphi \cdot \psi \, \mathrm{d}\Omega =: -\int_\Omega \varphi \cdot \mathcal{J}\psi \, \mathrm{d}\Omega, \qquad \forall \varphi, \psi \in C_c^\infty(\Omega).$$

Definition 5 (*Dirac Structure*)**.** Given a Hilbert space $\mathcal{E}$, called the effort space, and its topological dual[10] $\mathcal{F} := \mathcal{E}'$, called the flow space, we define the Bond space $\mathcal{B} := \mathcal{F} \times \mathcal{E}$ endowed with the bilinear symmetric product:

$$\left\langle\left\langle \begin{pmatrix} f^1 \\ e^1 \end{pmatrix}, \begin{pmatrix} f^2 \\ e^2 \end{pmatrix} \right\rangle\right\rangle_{\mathcal{B}} := \left\langle f^1, e^2 \right\rangle_{\mathcal{F},\mathcal{E}} + \left\langle f^2, e^1 \right\rangle_{\mathcal{F},\mathcal{E}},$$

where $\langle \cdot, \cdot \rangle_{\mathcal{F},\mathcal{E}}$ represents the duality bracket. A (Stokes-)Dirac structure is a subspace $\mathcal{D} \subset \mathcal{B}$ which is maximal isotropic in $\mathcal{B}$, *i.e.* it satisfies:

$$\mathcal{D}^\top = \mathcal{D},$$

where $\mathcal{D}^\top$ is the orthogonal companion of $\mathcal{D}$ in $\mathcal{B}$ with respect to the Bond product $\langle\langle \cdot, \cdot \rangle\rangle_{\mathcal{B}}$.

Remark 17. An important result in finite dimension is the kernel representation of a Dirac structure [133, § 5.1] which states that a Dirac structure always admits two matrices E and F of appropriate dimension such that:

$$\mathcal{D} = \left\{ \begin{pmatrix} f \\ e \end{pmatrix} \in \mathcal{B} \mid Ff + Ee = 0 \right\}.$$

After discretization, see Section 3, we are essentially concerned with the case $F^\top = F > 0$ and $E^\top = -E$ in the sequel. In that case, E is often denoted J and is call the structure matrix. We abuse the language and will talk about structure operator in the infinite-dimensional case.

Remark 18. In infinite dimensions, a Dirac structure is rather called a Stokes–Dirac structure, in order to emphasize that its structure operator is formally skew-symmetric thanks to the Stokes's divergence theorem.

[10] In finite dimension, the definition is often written in the other way: $\mathcal{E} := \mathcal{F}'$.

Remark 19. Rigorously, the Bond product makes use of the duality bracket between $\mathcal{E}$ and $\mathcal{F}$. In this work, we will always assume a strong regularity (*i.e.* at least C^1 in space and time) for the solutions to a pH system. In that case, this duality bracket reduces to a more convenient L^2-inner product over the spatial domain Ω. Moreover, the boundary traces of such solutions are then sufficiently regular to allow also the identification of the duality bracket at the boundary of Ω by the L^2-inner product at the boundary.

Appendix B. Proof of some theorems

B.1. Proof of Theorem 2

Along the trajectories of system (31), one has:

$$\begin{aligned}
\dot{\mathcal{H}} &= \int_\Omega \partial_t \boldsymbol{u} \cdot \delta_{\boldsymbol{u}} \mathcal{H} \mathrm{d}\,\Omega, \\
&= \int_\Omega \partial_t \boldsymbol{u} \cdot (\rho_0 \boldsymbol{u}) \mathrm{d}\,\Omega, \\
&= \int_\Omega \rho_0 \partial_t \boldsymbol{u} \cdot \boldsymbol{u} \mathrm{d}\,\Omega, \\
&= \int_\Omega \left(G(\boldsymbol{\omega}) \boldsymbol{u} \cdot \boldsymbol{u} - \mathbf{curl}(\boldsymbol{e}_c) \cdot \boldsymbol{u} + \mathbf{grad}(e_d) \cdot \boldsymbol{u} \right) \mathrm{d}\,\Omega, \\
&= \underbrace{\int_\Omega G(\boldsymbol{\omega}) \boldsymbol{u} \cdot \boldsymbol{u} \,\mathrm{d}\,\Omega}_{=0} - \int_\Omega \boldsymbol{e}_c \cdot \mathbf{curl}(\boldsymbol{u}) \mathrm{d}\,\Omega - \int_{\partial\Omega} \boldsymbol{e}_c \cdot (\boldsymbol{u} \wedge \boldsymbol{n}) \,\mathrm{d}\,\gamma \\
&\qquad - \int_\Omega e_d \underbrace{\mathrm{div}(\boldsymbol{u})}_{=0} \,\mathrm{d}\,\Omega + \int_{\partial\Omega} e_d \, \boldsymbol{u} \cdot \boldsymbol{n} \mathrm{d}\,\gamma, \\
&= - \int_\Omega \boldsymbol{e}_c \cdot \boldsymbol{f}_c \mathrm{d}\,\Omega - \int_{\partial\Omega} \boldsymbol{e}_c \cdot (\boldsymbol{u} \wedge \boldsymbol{n}) \,\mathrm{d}\,\gamma + \int_{\partial\Omega} e_d \, \boldsymbol{u} \cdot \boldsymbol{n} \mathrm{d}\,\gamma, \\
&= - \int_\Omega \boldsymbol{e}_c \cdot \boldsymbol{f}_c \mathrm{d}\,\Omega + \int_{\partial\Omega} \left(e_d \, \boldsymbol{u} \cdot \boldsymbol{n} - \boldsymbol{e}_c \cdot (\boldsymbol{u} \wedge \boldsymbol{n}) \right) \mathrm{d}\,\gamma, \\
&= - \int_\Omega \mu_c \, \|\boldsymbol{\omega}\|^2 \,\mathrm{d}\,\Omega \\
&\quad + \textstyle\int_{\partial\Omega} \left(\left(P + \frac{1}{2} \rho_0 \, \|\boldsymbol{u}\|^2 \right) \boldsymbol{u} \cdot \boldsymbol{n} - \mu_c \, \boldsymbol{\omega} \cdot (\boldsymbol{u} \wedge \boldsymbol{n}) \right) \mathrm{d}\,\gamma.
\end{aligned}$$

B.2. Proof of Theorem 6

Along the trajectories of system (36), one has:

$$\begin{aligned}
\dot{\mathcal{H}} &= \int_\Omega \rho_0 \, \partial_t \omega \, \delta_\omega^{\rho_0} \mathcal{H} \mathrm{d}\,\Omega, \\
&= \int_\Omega \rho_0 \, \partial_t \omega \, \psi \mathrm{d}\,\Omega, \\
&= \int_\Omega \left(J_\omega \psi - \mathrm{curl}_{2D} \mathbf{grad}^\perp(e_c) \right) \psi \mathrm{d}\,\Omega, \\
&= \int_\Omega \mathrm{curl}_{2D} \left(G(\omega) \, \mathbf{grad}^\perp(\psi) \right) \psi \mathrm{d}\,\Omega - \int_\Omega \mathrm{curl}_{2D} \mathbf{grad}^\perp(e_c) \, \psi \mathrm{d}\,\Omega, \\
&= \int_\Omega \underbrace{G(\omega) \, \mathbf{grad}^\perp(\psi) \cdot \mathbf{grad}^\perp(\psi)}_{=0} \mathrm{d}\,\Omega + \int_{\partial\Omega} \underbrace{\Theta G(\omega)}_{=\omega I_2} \mathbf{grad}^\perp(\psi) \cdot \boldsymbol{n} \, \psi \mathrm{d}\,\gamma \\
&\qquad - \int_\Omega \mathbf{grad}^\perp(e_c) \cdot \mathbf{grad}^\perp(\psi) \mathrm{d}\,\Omega - \int_{\partial\Omega} \Theta \mathbf{grad}^\perp(e_c) \cdot \boldsymbol{n} \, \psi \mathrm{d}\,\gamma, \\
&= \int_{\partial\Omega} \omega \, \psi \, \mathbf{grad}^\perp(\psi) \cdot \boldsymbol{n} \mathrm{d}\,\gamma - \int_\Omega \underbrace{e_c}_{=\mu_c \omega} \underbrace{\mathrm{curl}_{2D} \mathbf{grad}^\perp(\psi)}_{=\omega} \mathrm{d}\,\Omega \\
&\qquad + \int_{\partial\Omega} \underbrace{\Theta \mathbf{grad}^\perp(\psi)}_{=-\mathbf{grad}(\psi)} \cdot \boldsymbol{n} \, e_c \mathrm{d}\,\gamma - \int_{\partial\Omega} \underbrace{\mathcal{R} \mathbf{grad}^\perp(e_c)}_{=-\mathbf{grad}(\mu_c \, \omega)} \cdot \boldsymbol{n} \, \psi \mathrm{d}\,\gamma,
\end{aligned}$$

hence the result.

B.3. Proof of Theorem 8

First, note that, using the symmetry of the matrices $Q_{\boldsymbol{\alpha}}[\underline{h}(t)]$ and Q_h appearing in the definition of the discrete Hamiltonian $\mathcal{H}^d$ given in (43):

$$\begin{aligned}
\frac{\mathrm{d}}{\mathrm{d}t} \mathcal{H}^d(\underline{h}(t), \underline{\alpha}(t)) &= \underline{\alpha}(t)^\top \, Q_{\boldsymbol{\alpha}}[\underline{h}(t)] \, \frac{\mathrm{d}}{\mathrm{d}t} \underline{\alpha}(t) + \underline{h}(t)^\top \, Q_h \, \frac{\mathrm{d}}{\mathrm{d}t} \underline{h}(t) \\
&\quad + \frac{1}{2} \underline{\alpha}(t)^\top \, \frac{\mathrm{d}}{\mathrm{d}t} Q_{\boldsymbol{\alpha}}[\underline{h}(t)] \, \underline{\alpha}(t).
\end{aligned} \tag{74}$$

On the other hand, multiplying (41) by $\left(\underline{e_h}(t)^\top \; \underline{e_\alpha}(t)^\top \; \underline{e_\partial}(t)^\top \right)^\top$ by the left leads to:

$$\begin{aligned}
&\underline{e_h}(t)^\top \, M_h \, \frac{\mathrm{d}}{\mathrm{d}t} \underline{h}(t) + \underline{e_\alpha}(t)^\top \, M_\alpha \, \frac{\mathrm{d}}{\mathrm{d}t} \underline{\alpha}(t) - \underline{e_\partial}(t)^\top \, M_\partial \, \underline{f_\partial}(t) \\
&= \underline{e_h}(t)^\top \, D \, \underline{e_\alpha}(t) + \underline{e_h}(t)^\top \, B \, \underline{e_\partial}(t) - \underline{e_\alpha}(t)^\top \, D^\top \, \underline{e_h}(t) - \underline{e_\partial}(t)^\top \, B^\top \, \underline{e_h}(t),
\end{aligned}$$

which simplifies into:

$$\underline{e_h}(t)^\top \, M_h \, \frac{\mathrm{d}}{\mathrm{d}t} \underline{h}(t) + \underline{e_\alpha}(t)^\top \, M_\alpha \, \frac{\mathrm{d}}{\mathrm{d}t} \underline{\alpha}(t) = \underline{e_\partial}(t)^\top \, M_\partial \, \underline{f_\partial}(t).$$

Now, since the mass matrices are symmetric, one can make use of (42) to get:

$$\begin{aligned}
&\left(Q_h \, \underline{h}(t) + N[\underline{\alpha}(t)] \, \underline{\alpha}(t) \right)^\top \, \frac{\mathrm{d}}{\mathrm{d}t} \underline{h}(t) + \left(Q_{\boldsymbol{\alpha}}[\underline{h}(t)] \, \underline{\alpha}(t) \right)^\top \, \frac{\mathrm{d}}{\mathrm{d}t} \underline{\alpha}(t) \\
&= \underline{e_\partial}(t)^\top \, M_\partial \, \underline{f_\partial}(t),
\end{aligned}$$

or, after rearranging the terms and taking advantage of the symmetry of the Q matrices:

$$\begin{aligned}
&\underline{\alpha}(t)^\top \, N[\underline{\alpha}(t)]^\top \, \frac{\mathrm{d}}{\mathrm{d}t} \underline{h}(t) + \underline{h}(t)^\top \, Q_h \, \frac{\mathrm{d}}{\mathrm{d}t} \underline{h}(t) \\
&+ \underline{\alpha}(t)^\top \, Q_{\boldsymbol{\alpha}}[\underline{h}(t)] \, \frac{\mathrm{d}}{\mathrm{d}t} \underline{\alpha}(t) = \underline{e_\partial}(t)^\top \, M_\partial \, \underline{f_\partial}(t).
\end{aligned}$$

Combining the latter with (74) gives:

$$\begin{aligned}
&\frac{\mathrm{d}}{\mathrm{d}t} \mathcal{H}^d(\underline{h}(t), \underline{\alpha}(t)) = \underline{e_\partial}(t)^\top \, M_\partial \, \underline{f_\partial}(t) \\
&+ \frac{1}{2} \underline{\alpha}(t)^\top \, \frac{\mathrm{d}}{\mathrm{d}t} Q_{\boldsymbol{\alpha}}[\underline{h}(t)] \, \underline{\alpha}(t) - \underline{\alpha}(t)^\top \, N[\underline{\alpha}(t)]^\top \, \frac{\mathrm{d}}{\mathrm{d}t} \underline{h}(t).
\end{aligned}$$

Once again, the fact that the Hamiltonian is polynomial is crucial (compare the following with the equality in Remark 12), since it leads straightforwardly to:

$$\frac{1}{2} \underline{\alpha}(t)^\top \, \frac{\mathrm{d}}{\mathrm{d}t} Q_{\boldsymbol{\alpha}}[\underline{h}(t)] \, \underline{\alpha}(t) = \underline{\alpha}(t)^\top \, N[\underline{\alpha}(t)]^\top \, \frac{\mathrm{d}}{\mathrm{d}t} \underline{h}(t),$$

hence, to the result.

B.4. Proof of Theorem 10

Let us multiply (60) by $\left(\underline{\psi}^\top \; \underline{e_c}^\top \; \underline{u_n}^\top \; \underline{u_\tau}^\top \; \underline{\dot{u}_\tau}^\top \; \underline{y_c}^\top \right)^\top$ by the left. Then:

$$\underline{\psi}^\top \, M_\psi \, \underline{\dot{\psi}} + \underline{e_c}^\top \, M_c \, \underline{e_c} - \underline{u_n}^\top \, M_\partial \, \underline{y_n} - \underline{u_\tau}^\top \, M_\partial \, \underline{y_\tau} - \underline{\dot{u}_\tau}^\top \, M_\partial \, \underline{y_{\mathrm{d}t}} - \underline{y_c}^\top \, M_\partial \, \underline{u_c} = 0.$$

After rearrangement, it reads:

$$\underline{\psi}^\top \, M_\psi \, \underline{\dot{\psi}} - \underline{\dot{u}_\tau}^\top \, M_\partial \, \underline{y_{\mathrm{d}t}} = - \underline{e_c}^\top \, M_c \, \underline{e_c} + \underline{u_n}^\top \, M_\partial \, \underline{y_n} + \underline{u_\tau}^\top \, M_\partial \, \underline{y_\tau} + \underline{y_c}^\top \, M_\partial \, \underline{u_c}.$$

Now, with the discrete Hamiltonian $\mathcal{H}^d$, given in (61), let us show that $\frac{\mathrm{d}}{\mathrm{d}t} \mathcal{H}^d(\underline{\omega}) = \underline{\psi}^\top \, M_\psi \, \underline{\dot{\psi}} - \underline{\dot{u}_\tau}^\top \, M_\partial \, \underline{y_{\mathrm{d}t}}$. As in the continuous case, the difficulty relies on the fact that $\mathcal{H}^d$ is defined as a function of $\underline{\omega}$, hence:

$$\frac{\mathrm{d}}{\mathrm{d}t} \mathcal{H}^d(\underline{\omega}) = \nabla_{\underline{\omega}} \mathcal{H}^d(\underline{\omega}) \cdot \underline{\dot{\omega}},$$

and one requires to compute the gradient of the Hamiltonian with respect to the energy variable $\underline{\omega}$. Let us compute it in the distributional sense, following [106] at the continuous level, as in Proposition 4.

Let $\underline{w} \in \mathbb{R}^{N_c}$ be such that $w^d(\boldsymbol{\zeta}, t) = \sum_{k=1}^{N_c} w^k \, \boldsymbol{\Phi}^k(\boldsymbol{\zeta})$ is compactly supported and in the range of curl_{2D}, *i.e.*, there exists $\boldsymbol{\eta}^d \in \left(L^2(\Omega) \right)^2$ compactly supported and satisfying $\mathrm{curl}_{2D} \boldsymbol{\eta}^d = w^d$. Then, for all $\varepsilon > 0$:

$$\begin{aligned}
\frac{\mathcal{H}^d \left(\underline{\omega} + \varepsilon \underline{w} \right) - \mathcal{H}^d \left(\underline{\omega} \right)}{\varepsilon} &= \frac{1}{2\varepsilon} \int_\Omega \rho_0 \left\| \boldsymbol{u}^d + \varepsilon \boldsymbol{\eta}^d \right\|^2 \mathrm{d}\,\Omega \\
&\quad - \tfrac{1}{2\varepsilon} \textstyle\int_\Omega \rho_0 \, \left\| \boldsymbol{u}^d \right\|^2 \mathrm{d}\,\Omega, \\
&= \int_\Omega \rho_0 \, \boldsymbol{u}^d \cdot \boldsymbol{\eta}^d \mathrm{d}\,\Omega + O(\varepsilon).
\end{aligned}$$

Using $\boldsymbol{u}^d = \mathbf{grad}^\perp \left(\psi^d \right)$ and applying the integration by part (33) leads to:

$$\nabla_{\underline{\omega}} \mathcal{H}^d(\underline{\omega}) \cdot \underline{w} = \int_\Omega \rho_0 \, \psi^d w^d \mathrm{d}\,\Omega,$$

from which we recover that $\rho_0 \underline{\psi}$ is indeed the co-energy variable at the discrete level, as expected. Now:

$$\begin{aligned}
\nabla_{\underline{\omega}} \mathcal{H}^d(\underline{\omega}) \cdot \dot{\underline{\omega}} &= \int_\Omega \rho_0 \ \psi^d \partial_t \omega^d \, \mathrm{d}\,\Omega, \\
&= -\int_\Omega \rho_0 \ \psi^d \partial_t \left(\Delta \psi^d\right) \mathrm{d}\,\Omega, \\
&= -\int_\Omega \rho_0 \ \psi^d \Delta \left(\partial_t \psi^d\right) \mathrm{d}\,\Omega, \\
&= -\int_\Omega \rho_0 \ \psi^d \mathrm{div}\mathbf{grad}\left(\partial_t \psi^d\right) \mathrm{d}\,\Omega, \\
&= \int_\Omega \rho_0 \ \mathbf{grad}\left(\psi^d\right) \cdot \mathbf{grad}\left(\partial_t \psi^d\right) \mathrm{d}\,\Omega \\
&\qquad - \int_{\partial\Omega} \rho_0 \ \psi^d \ \mathbf{grad}\left(\partial_t \psi^d\right) \cdot \boldsymbol{n} \mathrm{d}\,\gamma, \\
&= \int_\Omega \rho_0 \ \mathbf{grad}\left(\psi^d\right) \cdot \mathbf{grad}\left(\partial_t \psi^d\right) \mathrm{d}\,\Omega - \int_{\partial\Omega} \rho_0 \ \psi^d \ \partial_t u_\tau \mathrm{d}\,\gamma, \\
&= \underline{\psi}^\top \ M_\psi \ \dot{\underline{\psi}} - \underline{\psi}^\top \ B_{\mathrm{d}t}^\top \ \dot{\underline{u}}_\tau,
\end{aligned}$$

hence the result, since $B_{\mathrm{d}t} \ \underline{\psi} = M_\partial \ \underline{y}_{\mathrm{d}t}$, and M_∂ is symmetric.

References

[1] Abhyankar S, Brown J, Constantinescu E, Ghosh D, Smith B, Zhang H. PETSc/TS: a modern scalable ODE/dAE solver library. Technical report, 2018, arXiv:1806.01437.

[2] Alonso A, Ydstie B, Banga J. From irreversible thermodynamics to a robust control theory for distributed process systems. J Process Control 2002;12:507–17. http://dx.doi.org/10.1016/S0959-1524(01)00017-8.

[3] Altmann R, Mehrmann V, Unger B. Port-Hamiltonian formulations of poroelastic network models. Math Comput Model Dyn Syst 2021;27:429–52. http://dx.doi.org/10.1080/13873954.2021.1975137.

[4] Altmann R, Schulze P. A port-Hamiltonian formulation of the Navier–Stokes equations for reactive flows. Systems Control Lett 2017;100:51–5. http://dx.doi.org/10.1016/j.sysconle.2016.12.005.

[5] Aoues S, Cardoso-Ribeiro F, Matignon D, Alazard D. Modeling and control of a rotating flexible spacecraft: A port-Hamiltonian approach. IEEE Trans Control Syst Technol 2017;27:355–62. http://dx.doi.org/10.1109/TCST.2017.2771244.

[6] Arnold D, Falk R, Winther R. Finite element exterior calculus, homological techniques, and applications. Acta Numer 2006;15:1–155. http://dx.doi.org/10.1017/S0962492906210018.

[7] Arnold D, Falk R, Winther R. Finite element exterior calculus: from hodge theory to numerical stability. Bull Amer Math Soc 2010;47:281–354. http://dx.doi.org/10.1090/s0273-0979-10-01278-4.

[8] Beattie C, Mehrmann V, Xu H, Zwart H. Linear port-Hamiltonian descriptor systems. Math Control Signals Systems 2018;30:1–27. http://dx.doi.org/10.1007/s00498-018-0223-3.

[9] Bendimerad-Hohl A, Haine G, Lefèvre L, Matignon D. Implicit port-Hamiltonian systems: structure-preserving discretization for the nonlocal vibrations in a viscoelastic nanorod, and for a seepage model. IFAC-PapersOnLine 2023a.;56:6789–95. http://dx.doi.org/10.1016/j.ifacol.2023.10.387, 22nd IFAC World Congress.

[10] Bendimerad-Hohl A, Haine G, Matignon D. Structure-preserving discretization of the cahn-hilliard equations recast as a port-Hamiltonian system. In: Geometric science of information. Cham: Springer; 2023b., p. 192–201. http://dx.doi.org/10.1007/978-3-031-38299-4_21.

[11] Bendimerad-Hohl A, Haine G, Matignon D, Maschke B. Structure-preserving discretization of a coupled allen-cahn and heat equation system. IFAC-PapersOnLine 2022;55:99–104. http://dx.doi.org/10.1016/j.ifacol.2022.08.037.

[12] Benner P, Goyal P, Van Dooren P. Identification of port-Hamiltonian systems from frequency response data. Systems Control Lett 2020;143:104741. http://dx.doi.org/10.1016/j.sysconle.2020.104741.

[13] Bird R. Transport phenomena. Appl Mech Rev 2002;55:R1–4. http://dx.doi.org/10.1115/1.1424298.

[14] Bochev P, Hyman J. Principles of mimetic discretizations of differential operators. In: Arnold D, Bochev P, Lehoucq R, Nicolaides R, Shashkov M, editors. Compatible spatial discretizations. IMA, vol. 142, Berlin: Springer Verlag; 2006, p. 89–119. http://dx.doi.org/10.1007/0-387-38034-5_5.

[15] Boffi D, Brezzi F, Fortin M. Mixed finite element methods and applications. Berlin, Heidelberg: Springer; 2015, http://dx.doi.org/10.1007/978-3-642-36519-5.

[16] Boyer F, Fabrie P. Mathematical tools for the study of the incompressible Navier–Stokes equations and related models. Applied mathematical sciences, vol. 183, New York: Springer; 2013, http://dx.doi.org/10.1007/978-1-4614-5975-0.

[17] Brayton R, Moser J. A theory of nonlinear networks. I. Quart Appl Math 1964;22:1–33.

[18] Brugnoli A, Alazard D, Pommier-Budinger V, Matignon D. Port-Hamiltonian formulation and symplectic discretization of plate models part I: Mindlin model for thick plates. Appl Math Model 2019a;75:940–60. http://dx.doi.org/10.1016/j.apm.2019.04.035.

[19] Brugnoli A, Alazard D, Pommier-Budinger V, Matignon D. Port-Hamiltonian formulation and symplectic discretization of plate models part II: Kirchhoff model for thin plates. Appl Math Model 2019b;75:961–81. http://dx.doi.org/10.1016/j.apm.2019.04.036.

[20] Brugnoli A, Cardoso-Ribeiro F, Haine G, Kotyczka P. Partitioned finite element method for structured discretization with mixed boundary conditions. IFAC-PapersOnLine 2020;53:7557–62. http://dx.doi.org/10.1016/j.ifacol.2020.12.1351, 21st IFAC World Congress..

[21] Brugnoli A, Haine G, Matignon D. Explicit structure-preserving discretization of port-Hamiltonian systems with mixed boundary control. IFAC-PapersOnLine 2022a;55:418–23. http://dx.doi.org/10.1016/j.ifacol.2022.11.089, 25th International Symposium on Mathematical Theory of Networks and Systems MTNS 2022.

[22] Brugnoli A, Haine G, Matignon D. Stokes-Dirac structures for distributed parameter port-Hamiltonian systems: An analytical viewpoint. Commun Anal Mech 2023;15:362–87. http://dx.doi.org/10.3934/cam.2023018.

[23] Brugnoli A, Haine G, Serhani A, Vasseur X. Numerical approximation of port-Hamiltonian systems for hyperbolic or parabolic PDEs with boundary control. J Appl Math Phys 2021;9:1278–321. http://dx.doi.org/10.4236/jamp.2021.96088, supplementary material 10.5281/zenodo.3938600.

[24] Brugnoli A, Rashad R, Stramigioli S. Dual field structure-preserving discretization of port-Hamiltonian systems using finite element exterior calculus. J Comput Phys 2022b;471:111601. http://dx.doi.org/10.1016/j.jcp.2022.111601.

[25] Califano F, Rashad R, Schuller F, Stramigioli S. Geometric and energy-aware decomposition of the Navier–Stokes equations: A port-Hamiltonian approach. Phys Fluids 2021;33:047114. http://dx.doi.org/10.1063/5.0048359.

[26] Califano F, Rashad R, Schuller F, Stramigioli S. Energetic decomposition of distributed systems with moving material domains: the port-Hamiltonian model of fluid–structure interaction. J Geom Phys 2022a;175:104477. http://dx.doi.org/10.1016/j.geomphys.2022.104477.

[27] Califano F, Rashad R, Stramigioli S. A differential geometric description of thermodynamics in continuum mechanics with application to Fourier–Navier–Stokes fluids. Phys Fluids 2022b;34:107113. http://dx.doi.org/10.1063/5.0119517.

[28] Cardoso-Ribeiro F, Brugnoli A, Matignon D, Lefèvre L. Port-Hamiltonian modeling, discretization and feedback control of a circular water tank. In: 2019 IEEE 58th conference on decision and control. 2019, p. 6881–6. http://dx.doi.org/10.1109/CDC40024.2019.9030007.

[29] Cardoso-Ribeiro F, Haine G, Lefèvre L, Matignon D. Rotational shallow water equations with viscous damping and boundary control: structure-preserving spatial discretization. 2023, http://dx.doi.org/10.21203/rs.3.rs-3006274/v2, PREPRINT Available at Research Square.

[30] Cardoso-Ribeiro F, Matignon D, Lefèvre L. A Partitioned Finite-Element Method for power-preserving discretization of open systems of conservation laws. IMA J Math Control Inf 2021a;38:493–533. http://dx.doi.org/10.1093/imamci/dnaa038.

[31] Cardoso-Ribeiro F, Matignon D, Lefèvre L. Dissipative shallow water equations: a port-Hamiltonian formulation. IFAC-PapersOnLine 2021b;54:167–72. http://dx.doi.org/10.1016/j.ifacol.2021.11.073, 7th IFAC Workshop on Lagrangian and Hamiltonian Methods for Nonlinear Control LHMNC 2021.

[32] Cardoso-Ribeiro F, Matignon D, Pommier-Budinger V. A port-Hamiltonian model of liquid sloshing in moving containers and application to a fluid–structure system. J Fluids Struct 2017;69:402–27. http://dx.doi.org/10.1016/j.jfluidstructs.2016.12.007.

[33] Cardoso-Ribeiro F, Matignon D, Pommier-Budinger V. Port-Hamiltonian model of two-dimensional shallow water equations in moving containers. IMA J Math Control Inform 2020;37:1348–66. http://dx.doi.org/10.1093/imamci/dnaa016.

[34] Cervera J, van der Schaft A, Baños A. Interconnection of port-Hamiltonian systems and composition of Dirac structures. Automatica 2007;43:212–25. http://dx.doi.org/10.1016/j.automatica.2006.08.014.

[35] Chorin A, Marsden J. A mathematical introduction to fluid mechanics. Texts in applied mathematics, vol. 4, New York: Springer; 1992, http://dx.doi.org/10.1007/978-1-4612-0883-9.

[36] Cisneros N, Rojas A, Ramirez H. Port-Hamiltonian modeling and control of a micro-channel experimental plant. IEEE Access 2020;8:176935–46. http://dx.doi.org/10.1109/ACCESS.2020.3026653.

[37] Cotter C. Compatible finite element methods for geophysical fluid dynamics. Acta Numer 2023;32:291–393. http://dx.doi.org/10.1017/S0962492923000028.

[38] Courant T. Dirac manifolds. Trans Amer Math Soc 1990;319:631–61. http://dx.doi.org/10.1090/S0002-9947-1990-0998124-1.

[39] De Groot S, Mazur P. Non-equilibrium thermodynamics. Courier Corporation; 2013.

[40] Diab M, Tischendorf C. Splitting methods for linear circuit DAEs of index 1 in port-Hamiltonian form. In: van Beurden M, Budko N, Schilders W, editors. Scientific computing in electrical engineering. Cham: Springer International Publishing; 2021, p. 211–9. http://dx.doi.org/10.1007/978-3-030-84238-3_21.

[41] Domschke P, Hiller B, Lang J, Mehrmann V, Morandin R, Tischendorf C. Gas network modeling: an overview. Technical report, Technische Universität Darmstadt.; 2021, URL https://opus4.kobv.de/opus4-trr154/frontdoor/index/index/docId/411.

[42] Dubljevic S. Quo vadis advanced chemical process control. Can J Chem Eng 2022;100(2135). http://dx.doi.org/10.1002/cjce.24505.

[43] Duindam V, Macchelli A, Stramigioli S, Bruyninckx H. Modeling and control of complex physical systems: the port-Hamiltonian approach. Berlin, Heidelberg: Springer; 2009, http://dx.doi.org/10.1007/978-3-642-03196-0.

[44] Eberard D, Maschke B, van der Schaft A. An extension of Hamiltonian systems to the thermodynamic phase space: Towards a geometry of nonreversible processes. Rep Math Phys 2007;60:175–98. http://dx.doi.org/10.1016/S0034-4877(07)00024-9.

[45] Edwards B, Öttinger H, Jongschaap R. On the relationships between thermodynamic formalisms for complex fluids. J Non-Equilib Thermodyn 1997;22:356–73. http://dx.doi.org/10.1515/jnet.1997.22.4.356.

[46] Egger H. Structure preserving approximation of dissipative evolution problems. Numer Math 2019;143:85–106. http://dx.doi.org/10.1007/s00211-019-01050-w.

[47] Emmrich E, Mehrmann V. Operator differential–algebraic equations arising in fluid dynamics. Comput Methods Appl Math 2013;13:443–70. http://dx.doi.org/10.1515/cmam-2013-0022.

[48] Erbay M, Jacob B, Morris K. On the weierstraß form of infinite dimensional differential algebraic equations. 2024, arXiv:2402.17560.

[49] Erbay M, Jacob B, Morris K, Reis T, Tischendorf C. Index concepts for linear differential–algebraic equations in finite and infinite dimensions. 2024, arXiv:2401.01771.

[50] Farle O, Baltes R, Dyczij-Edlinger R. A port-Hamiltonian finite-element formulation for the transmission line. In: Proceedings of the 21st International Symposium on Mathematical Theory of Networks and Systems. 2014a, p. 724–8.

[51] Farle O, Baltes R, Dyczij-Edlinger R. Strukturerhaltende diskretisierung verteilt-parametrischer port-hamiltonscher systeme mittels finiter elemente. at-Automatisierungstechnik 2014b;62:500–11. http://dx.doi.org/10.1515/auto-2014-1093.

[52] Farle O, Klis D, Jochum M, Floch O, Dyczij-Edlinger R. A port-Hamiltonian finite-element formulation for the maxwell equations. In: 2013 International conference on electromagnetics in advanced applications. IEEE; 2013, p. 324–7. http://dx.doi.org/10.1109/ICEAA.2013.6632246.

[53] Ferrarro G, Fournié M, Haine G. Simulation and control of interactions in multi-physics, a Python package for port-Hamiltonian systems. In: Proceedings of the 8th IFAC Workshop on Lagrangian and Hamiltonian Methods for Non Linear Control (LHMNC). Besançon, France; 2024.

[54] Gawlik E, Gay-Balmaz F. A variational finite element discretization of compressible flow. Found Comput Math 2021;21:961–1001. http://dx.doi.org/10.1007/s10208-020-09473-w.

[55] Gay-Balmaz F, Yoshimura H. A variational formulation of nonequilibrium thermodynamics for discrete open systems with mass and heat transfer. Entropy 2018;20(163). http://dx.doi.org/10.3390/e20030163.

[56] Gerbeau J, Perthame B. Derivation of viscous saint-venant system for laminar shallow water; numerical validation. Discr Contin Dyn Syst - B 2001;1:89–102. http://dx.doi.org/10.3934/dcdsb.2001.1.89.

[57] Geuzaine C, Remacle J. Gmsh: A 3-D finite element mesh generator with built-in pre- and post-processing facilities. Internat J Numer Methods Engrg 2009;79:1309–31. http://dx.doi.org/10.1002/nme.2579.

[58] Ghia U, Ghia K, Shin C. High-re solutions for incompressible flow using the Navier–Stokes equations and a multigrid method. J Comput Phys 1982;48:387–411. http://dx.doi.org/10.1016/0021-9991(82)90058-4.

[59] Girault V, Raviart P. Finite element methods for Navier–Stokes equations. Berlin, Heidelberg: Springer; 2011, http://dx.doi.org/10.1007/978-3-642-61623-5.

[60] Golo G, Talasila V, van der Schaft A, Maschke B. Hamiltonian discretization of boundary control systems. Automatica 2004;40:757–71. http://dx.doi.org/10.1016/j.automatica.2003.12.017.

[61] Grmela M. Lagrange hydrodynamics as extended Euler hydrodynamics: Hamiltonian and GENERIC structures. Phys Lett A 2002;296:97–104. http://dx.doi.org/10.1016/S0375-9601(02)00190-1.

[62] Grmela M, Öttinger H. Dynamics and thermodynamics of complex fluids. I. Development of a general formalism. Phys Rev E 1997;56:6620–32. http://dx.doi.org/10.1103/PhysRevE.56.6620.

[63] Gugercin S, Polyuga R, Beattie C, van der Schaft A. Structure-preserving tangential interpolation for model reduction of port-Hamiltonian systems. Automatica 2012;48:1963–74. http://dx.doi.org/10.1016/j.automatica.2012.05.052, URL https://www.sciencedirect.com/science/article/pii/S0005109812002257.

[64] Haine G, Matignon D. Incompressible Navier–Stokes equation as port-Hamiltonian systems: velocity formulation versus vorticity formulation. IFAC-PapersOnLine 2021;54:161–6. http://dx.doi.org/10.1016/j.ifacol.2021.11.072, 7th IFAC Workshop on Lagrangian and Hamiltonian Methods for Nonlinear Control LHMNC 2021.

[65] Haine G, Matignon D, Monteghetti F. Long-time behavior of a coupled heat-wave system using a structure-preserving finite element method. Math Rep 2022a;24(74):187–215.

[66] Haine G, Matignon D, Monteghetti F. Structure-preserving discretization of maxwell's equations as a port-Hamiltonian system. IFAC-PapersOnLine 2022b;55:424–9. http://dx.doi.org/10.1016/j.ifacol.2022.11.090, 25th International Symposium on Mathematical Theory of Networks and Systems MTNS 2022.

[67] Haine G, Matignon D, Serhani A. Numerical analysis of a structure-preserving space-discretization for an anisotropic and heterogeneous boundary controlled N-dimensional wave equation as a port-Hamiltonian system. Int J Numer Anal Model 2023;20:92–133. http://dx.doi.org/10.4208/ijnam2023-1005.

[68] Hamroun B, Dimofte A, Lefèvre L, Mendes E. Control by interconnection and energy-shaping methods of port Hamiltonian models, application to the shallow water equations. Eur J Control 2010;16:545–63. http://dx.doi.org/10.3166/ejc.16.545-563.

[69] Hamroun B, Lefèvre L, Mendes E. Port-based modelling for open channel irrigation systems. Trans Fluid Mech 2006;1:995–1009.

[70] Heidari H, Zwart H. Port-Hamiltonian modelling of nonlocal longitudinal vibrations in a viscoelastic nanorod. Math Comput Model Dyn Syst 2019;25:447–62. http://dx.doi.org/10.1080/13873954.2019.1659374.

[71] Hiemstra R, Toshniwal D, Huijsmans R, Gerritsma M. High order geometric methods with exact conservation properties. J Comput Phys 2014;257:1444–71. http://dx.doi.org/10.1016/j.jcp.2013.09.027.

[72] Jacob B, Morris K. On solvability of dissipative partial differential–algebraic equations. IEEE Control Syst Lett 2022;6:3188–93. http://dx.doi.org/10.1109/LCSYS.2022.3183479.

[73] Jacob B, Zwart H. Linear port-Hamiltonian systems on infinite-dimensional spaces. Basel: Birkhäuser; 2012, http://dx.doi.org/10.1007/978-3-0348-0399-1.

[74] Jongschaap R. The matrix model, a driven state variables approach to non-equilibrium thermodynamics. J Non-Newton Fluid Mech 2001;96:63–76. http://dx.doi.org/10.1016/S0377-0257(00)00136-1.

[75] Jongschaap R, Öttinger H. The mathematical representation of driven thermodynamic systems. J Non-Newton Fluid Mech 2004;120:3–9. http://dx.doi.org/10.1016/j.jnnfm.2003.11.008, 3rd International workshop on Nonequilibrium Thermodynamics and Complex Fluids.

[76] Kotyczka P. Numerical methods for distributed parameter port-Hamiltonian systems. TUM.University Press; 2019, http://dx.doi.org/10.14459/2019md1510230.

[77] Kotyczka P, Maschke B, Lefèvre L. Weak form of Stokes–Dirac structures and geometric discretization of port-Hamiltonian systems. J Comput Phys 2018;361:442–76. http://dx.doi.org/10.1016/j.jcp.2018.02.006.

[78] Kraus M. Metriplectic integrators for dissipative fluids. In: Geometric science of information. Cham: Springer; 2021, p. 292–301. http://dx.doi.org/10.1007/978-3-030-80209-7_33.

[79] Kunkel P, Mehrmann V. Differential-algebraic equations: Analysis and numerical solution. In: EMS textbooks in mathematics. Zürich: European Mathematical Society; 2006, http://dx.doi.org/10.4171/017.

[80] Kurula M, Zwart H. Linear wave systems on n-d spatial domains. Internat J Control 2015;88:1063–77. http://dx.doi.org/10.1080/00207179.2014.993337.

[81] Lagrée P. Equations de saint venant et application aux mouvements de fonds érodables. 2021, URL http://www.lmm.jussieu.fr/%7Elagree/COURS/MFEnv/MFEnv.pdf. class notes.

[82] Lamour R, März R, Tischendorf C. Abstract differential–algebraic equations. Berlin, Heidelberg: Springer Berlin Heidelberg; 2013, p. 539–80. http://dx.doi.org/10.1007/978-3-642-27555-5_12.

[83] Le Gorrec Y, Zwart H, Maschke B. Dirac Structures and Boundary Control Systems Associated with Skew-Symmetric Differential Operators. SIAM J Control Optim 2005;44:1864–92. http://dx.doi.org/10.1137/040611677.

[84] Lequeurre J, Munnier A. Vorticity and stream function formulations for the 2D Navier–Stokes equations in a bounded domain. J Math Fluid Mech 2020;22:15. http://dx.doi.org/10.1007/s00021-019-0479-5.

[85] Logg A, Mardal K, Wells G. Automated solution of differential equations by the finite element method. Berlin, Heidelberg: Springer; 2012, http://dx.doi.org/10.1007/978-3-642-23099-8.

[86] Lohmayer M, Kotyczka P, Leyendecker S. Exergetic port-Hamiltonian systems: modelling basics. Math Comput Model Dyn Syst 2021;27:489–521. http://dx.doi.org/10.1080/13873954.2021.1979592.

[87] Lopes N, Hélie T. Energy balanced model of a jet interacting with a brass player's lip. Acta Acust United Acust 2016;102:141–54. http://dx.doi.org/10.3813/AAA.918931.

[88] Marche F. Derivation of a new two-dimensional viscous shallow water model with varying topography, bottom friction and capillary effects. Eur J Mech B/Fluids 2007;26:49–63. http://dx.doi.org/10.1016/j.euromechflu.2006.04.007.

[89] Maschke B, van der Schaft A. Linear boundary port Hamiltonian systems defined on Lagrangian submanifolds. IFAC-PapersOnLine 2020;53:7734–9. http://dx.doi.org/10.1016/j.ifacol.2020.12.1526, 21st IFAC World Congress 2020.

[90] Mehrmann V, Unger B. Control of port-Hamiltonian differential–algebraic systems and applications. Acta Numer 2023;32:395–515. http://dx.doi.org/10.1017/S0962492922000083.

[91] Mehrmann V, van der Schaft A. Differential–algebraic systems with dissipative Hamiltonian structure. Math Control Signals Systems 2023;35:541–84. http://dx.doi.org/10.1007/s00498-023-00349-2.

[92] Mehrmann V, Zwart H. Abstract dissipative Hamiltonian differential–algebraic equations are everywhere. 2024, arXiv:2311.03091.

[93] Merker J, Krüger M. On a variational principle in thermodynamics. Contin Mech Thermodyn 2013;25:779–93. http://dx.doi.org/10.1007/s00161-012-0277-2.

[94] Mohamed M, Hirani A, Samtaney R. Discrete exterior calculus discretization of incompressible Navier–Stokes equations over surface simplicial meshes. J Comput Phys 2016;312:175–91. http://dx.doi.org/10.1016/j.jcp.2016.02.028.

[95] Mora L, Le Gorrec Y, Matignon D, Ramirez H. Irreversible port-Hamiltonian modelling of 3D compressible fluids. IFAC-PapersOnLine 2023;56:6394–9. http://dx.doi.org/10.1016/j.ifacol.2023.10.836, 22nd IFAC World Congress.

[96] Mora L, Le Gorrec Y, Matignon D, Ramirez H, Yuz J. On port-Hamiltonian formulations of 3-dimensional compressible Newtonian fluids. Phys Fluids 2021;33:117117. http://dx.doi.org/10.1063/5.0067784.

[97] Mora L, Ramirez H, Yuz J, Le Gorrec Y, Zañartu M. Energy-based fluid–structure model of the vocal folds. IMA J Math Control Inform 2020a;38:466–92. http://dx.doi.org/10.1093/imamci/dnaa031.

[98] Mora L, Yann L, Ramirez H, Yuz J. Fluid-structure port-Hamiltonian model for incompressible flows in tubes with time varying geometries. Math Comput Model Dyn Syst 2020b;26:409–33. http://dx.doi.org/10.1080/13873954.2020.1786841.

[99] Morandin R. Modeling and numerical treatment of port-Hamiltonian descriptor systems, doctorate. Technische Universität Berlin; 2024, URL https://depositonce.tu-berlin.de/items/e9b3d954-dd50-48b0-85ce-9e9743d87479.

[100] Morrison P. Bracket formulation for irreversible classical fields. Phys Lett A 1984;100:423–7. http://dx.doi.org/10.1016/0375-9601(84)90635-2.

[101] Morrison P. Hamiltonian description of the ideal fluid. Rev Modern Phys 1998;70:467–521. http://dx.doi.org/10.1103/RevModPhys.70.467.

[102] Moses Badlyan A, Maschke B, Beattie C, Mehrmann V. Open physical systems: From GENERIC to port-Hamiltonian systems. In: Mathematical theory of networks and systems. Hong Kong, China; 2018, p. 204–11.

[103] Moulla R, Lefèvre L, Maschke B. Pseudo-spectral methods for the spatial symplectic reduction of open systems of conservation laws. J Comput Phys 2012;231:1272–92. http://dx.doi.org/10.1016/j.jcp.2011.10.008.

[104] Mrugala R, Nulton J, Schon J, Salamon P. Contact structure in thermodynamic theory. Rep Math Phys 1991;29:109–21. http://dx.doi.org/10.1016/0034-4877(91)90017-H.

[105] Ngoc Minh Trang Vu L, Maschke B. A structured control model for the thermo-magneto-hydrodynamics of plasmas in tokamaks. Math Comput Model Dyn Syst 2016;22:181–206. http://dx.doi.org/10.1080/13873954.2016.1154874.

[106] Olver P. Applications of Lie groups to differential equations. Graduate texts in mathematics, 2nd ed.. vol. 107, New York: Springer-Verlag; 1993, http://dx.doi.org/10.1007/978-1-4684-0274-2.

[107] Öttinger H. Generic integrators: Structure preserving time integration for thermodynamic systems. J Non-Equilib Thermodyn 2018;43:89–100. http://dx.doi.org/10.1515/jnet-2017-0034.

[108] Öttinger H, Grmela M. Dynamics and thermodynamics of complex fluids. II. Illustrations of a general formalism. Phys Rev E 1997;56:6633–55. http://dx.doi.org/10.1103/PhysRevE.56.6633.

[109] Pasumarthy R, Ambati V, van der Schaft A. Port-Hamiltonian formulation of shallow water equations with coriolis force and topography. In: Mathematical theory of networks and systems. VA, USA: Blacksburg; 2008.

[110] Pasumarthy R, Ambati V, van der Schaft A. Port-Hamiltonian discretization for open channel flows. Systems Control Lett 2012;61:950–8. http://dx.doi.org/10.1016/j.sysconle.2012.05.003.

[111] Payen G, Matignon D, Haine G. Modelling and structure-preserving discretization of maxwell's equations as port-Hamiltonian system. IFAC-PapersOnLine 2020;53:7581–6. http://dx.doi.org/10.1016/j.ifacol.2020.12.1355, 21st IFAC World Congress.

[112] Philipp F, Reis T, Schaller M. Infinite-dimensional port-Hamiltonian systems – a system node approach. 2023, arXiv:2302.05168.

[113] Ramirez H, Le Gorrec Y. An irreversible port-Hamiltonian formulation of distributed diffusion processes. IFAC-PapersOnLine 2016;49:46–51. http://dx.doi.org/10.1016/j.ifacol.2016.10.752, 2th IFAC Workshop on Thermodynamic Foundations for a Mathematical Systems Theory TFMST 2016.

[114] Ramirez H, Le Gorrec Y. An overview on irreversible port-Hamiltonian systems. Entropy 2022;24(1478). http://dx.doi.org/10.3390/e24101478.

[115] Ramirez H, Le Gorrec B. Boundary controlled irreversible port-Hamiltonian systems. Chem Eng Sci 2022;248:117107. http://dx.doi.org/10.1016/j.ces.2021.117107.

[116] Ramirez H, Maschke B, Sbarbaro D. Irreversible port-Hamiltonian systems: A general formulation of irreversible processes with application to the CSTR. Chem Eng Sci 2013;89:223–34. http://dx.doi.org/10.1016/j.ces.2012.12.002.

[117] Rashad R, Califano F, Schuller F, Stramigioli S. Port-Hamiltonian modeling of ideal fluid flow: Part I. Foundations and kinetic energy. J Geom Phys 2021a;164:104201. http://dx.doi.org/10.1016/j.geomphys.2021.104201.

[118] Rashad R, Califano F, Schuller F, Stramigioli S. Port-Hamiltonian modeling of ideal fluid flow: Part II. Compressible and incompressible flow. J Geom Phys 2021b;164:104199. http://dx.doi.org/10.1016/j.geomphys.2021.104199.

[119] Rashad R, Califano F, van der Schaft A, Stramigioli S. Twenty years of distributed port-Hamiltonian systems: a literature review. IMA J Math Control Inform 2020;37:1400–22. http://dx.doi.org/10.1093/imamci/dnaa018.

[120] Reis T, Schaller M. Port-Hamiltonian formulation of oseen flows. 2023, arXiv:2305.09618.

[121] Rettberg J, Wittwar D, Buchfink P, Brauchler A, Ziegler P, Fehr J, et al. Port-Hamiltonian fluid–structure interaction modelling and structure-preserving model order reduction of a classical guitar. Math Comput Model Dyn Syst 2023;29:116–48. http://dx.doi.org/10.1080/13873954.2023.2173238.

[122] Schiebl M, Betsch P. Structure-preserving space–time discretization of large-strain thermo-viscoelasticity in the framework of GENERIC. Internat J Numer Methods Engrg 2021;122:3448–88. http://dx.doi.org/10.1002/nme.6670.

[123] Serhani A, Matignon D, Haine G. A partitioned finite element method for the structure-preserving discretization of damped infinite-dimensional port-Hamiltonian systems with boundary control. In: Geometric science of information. Springer, Cham; 2019, p. 549–58. http://dx.doi.org/10.1007/978-3-030-26980-7_57.

[124] Serhani A, Matignon D, Haine G. Anisotropic heterogeneous n-d heat equation with boundary control and observation: II. Structure-preserving discretization. IFAC-PapersOnLine 2019b;52:57–62. http://dx.doi.org/10.1016/j.ifacol.2019.07.009, 3rd IFAC Workshop on Thermodynamic Foundations for a Mathematical Systems Theory (TFMST 2019)..

[125] Serhani A, Matignon D, Haine G. Partitioned finite element method for port-Hamiltonian systems with boundary damping: Anisotropic heterogeneous 2D wave equations. IFAC-PapersOnLine 2019c;52:96–101. http://dx.doi.org/10.1016/j.ifacol.2019.08.017, 3rd IFAC Workshop on Control of Systems Governed by Partial Differential Equations CPDE 2019.

[126] Seslija M, van der Schaft J. Discrete exterior geometry approach to structure-preserving discretization of distributed-parameter port-Hamiltonian systems. J Geom Phys 2012;62:1509–31. http://dx.doi.org/10.1016/j.geomphys.2012.02.006.

[127] Skrepek N. Well-posedness of linear first order port-Hamiltonian systems on multidimensional spatial domains. Evolut Equ Control Theory 2021;10:965–1006. http://dx.doi.org/10.3934/eect.2020098.

[128] Temam R. Navier–Stokes equations: theory and numerical analysis. Revised ed.. American Mathematical Society; 2001.

[129] Thuburn J, Cotter C. A primal–dual mimetic finite element scheme for the rotating shallow water equations on polygonal spherical meshes. J Comput Phys 2015;290:274–97. http://dx.doi.org/10.1016/j.jcp.2015.02.045.

[130] Trenchant V, Ramirez H, Le Gorrec Y, Kotyczka P. Finite differences on staggered grids preserving the port-Hamiltonianz structure with application to an acoustic duct. J Comput Phys 2018;373:673–97. http://dx.doi.org/10.1016/j.jcp.2018.06.051.

[131] van der Schaft A. port-Hamiltonian differential-algebraic systems. Berlin, Heidelberg: Springer; 2013, p. 173–226. http://dx.doi.org/10.1007/978-3-642-34928-7_5.

[132] van der Schaft A. Classical thermodynamics revisited: A systems and control perspective. IEEE Control Syst Mag 2021;41:32–60.

[133] van der Schaft A, Jeltsema D. Port-Hamiltonian systems theory: An introductory overview. Found Trends Syst Control 2014;1:173–378. http://dx.doi.org/10.1561/2600000002.

[134] van der Schaft A, Maschke B. On the Hamiltonian formulation of nonholonomic mechanical systems. Rep Math Phys 1994;34:225–33.

[135] van der Schaft A, Maschke B. Hamiltonian formulation of distributed-parameter systems with boundary energy flow. J Geom Phys 2002;42:166–94. http://dx.doi.org/10.1016/S0393-0440(01)00083-3.

[136] van der Schaft A, Maschke B. Generalized port-Hamiltonian DAE systems. Systems Control Lett 2018a;121:31–7. http://dx.doi.org/10.1016/j.sysconle.2018.09.008.

[137] van der Schaft A, Maschke B. Geometry of thermodynamic processes. Entropy 2018b;20(925). http://dx.doi.org/10.3390/e20120925.

[138] van der Schaft A, Mehrmann V. Linear port-Hamiltonian DAE systems revisited. Systems Control Lett 2023;177:105564. http://dx.doi.org/10.1016/j.sysconle.2023.105564.

[139] Villegas J, Le Gorrec Y, Zwart H, Maschke B. Boundary control for a class of dissipative differential operators including diffusion systems. In: Mathematical theory of networks and systems. Kyoto, Japan Kyoto, Japan; 2006, p. 24–8.

[140] Vu N, Lefèvre L, Maschke B. Geometric spatial reduction for port-Hamiltonian systems. Systems Control Lett 2019;125:1–8. http://dx.doi.org/10.1016/j.sysconle.2019.01.002.

[141] Vu N, Lefèvre L, Nouailletas R, Brémond S. Symplectic spatial integration schemes for systems of balance equations. J Process Control 2017;51:1–17. http://dx.doi.org/10.1016/j.jprocont.2016.12.005.

[142] Warsewa A, Böhm M, Sawodny O, Tarín C. A port-Hamiltonian approach to modeling the structural dynamics of complex systems. Appl Math Model 2021;89:1528–46. http://dx.doi.org/10.1016/j.apm.2020.07.038.

[143] Zhang Y, Palha A, Gerritsma M, Rebholz L. A mass-, kinetic energy- and helicity-conserving mimetic dual-field discretization for three-dimensional incompressible Navier–Stokes equations, part I: Periodic domains. J Comput Phys 2022;451:110868. http://dx.doi.org/10.1016/j.jcp.2021.110868.